Nano Research
2023, 16(12): 12983–13007
ISSN 1998-0124 CN 11-5974/O4
https://doi.org/10.1007/s12274-023-6239-4

Review Article

Electrodes for Li-ion batteries: From high-voltage $LiCoO_2$ to Co-reduced /Co-free layered oxides with potential anodes

Luting Song[1] and Weiguo Chu[1,2] (✉)

[1] *Nanofabrication Laboratory, National Center for Nanoscience and Technology, Beijing 100190, China*
[2] *Center of Materials Science and Optoelectronics Engineering, University of Chinese Academy of Sciences, Beijing 100049, China*

© Tsinghua University Press 2023

Received: 30 June 2023 / **Revised:** 23 September 2023 / **Accepted:** 3 October 2023

ABSTRACT

Li-ion batteries (LIBs) are one type of more and more widely used devices for energy storage and power supply in which cathode materials are playing a relatively more decisive role at current stage. In this review, we start with pioneeringly commercialized $LiCoO_2$ (LCO) with a layered rhombohedral structure (space group $R\bar{3}m$) to discuss novel sequentially emerging LCO-derived layered oxides from the perspectives of both cobalt content reduction and performance improvement. Emphasis is placed on the improvement of high-voltage performance of LCO and Co-reduced/free layered oxides, including Co-reduced high-nickel layered oxides, Co-free Li-rich layered oxides, and Ni-based layered oxides cathodes, and their underlying mechanisms via different strategies. Also, possibly matched carbon and silicon-based anode materials are briefly discussed. The common issues and prospects of the layered oxides cathodes and their potential anodes are summarized and commented on. This review can help understand the emergence logics of novel layered oxides with gradually vanishing cobalt involved, provide insights about the underlying mechanisms of performance enhancement pertaining to particular strategies, and even inspire the discovery of novel cathode materials with high performance and low cost.

KEYWORDS

Li-ion batteries, cathodic materials, anode materials, high-voltage $LiCoO_2$, Co-reduced/free layered oxides

1 Introduction

The adverse effects of greenhouse gases on climate change are well recognized world-wide, which requires to develop novel green energy-generated technologies (solar, wind, etc.) [1, 2]. With their emergence, corresponding energy storage solutions need to be proposed as well. Rechargeable lithium-ion batteries (LIBs) as a very important energy storage technology play a critical role in power supply for electric vehicles (EVs), portable electronics, tools, etc. General Motors and Ford as two largest vehicle suppliers from the U.S. plan to end the production of engine-powered cars and will exclusively supply EVs by 2035 [1]. Therefore, high performance and low cost rechargeable LIBs as highly efficient power supplies for EVs, and portable electronics and tools will still be the focus of interest for energy storage technologies in the coming years [3, 4].

Lithium transition metal oxides ($LiTMO_2$) cathodes are playing an increasingly important role in LIBs for power supply as a result of high energy density and superior round-trip efficiency [5–7]. To achieve a high energy density, efforts have been focused on electrochemical activation of transition metal as much as possible as an active redox center by carefully designing chemical constituents in layered oxides [8–10]. As a pioneeringly commercialized cathode material in 1991, $LiCoO_2$ (LCO) still shows a relatively low practical capacity of about 175 mAh·g^{-1} despite a high theoretical capacity of 274 mAh·g^{-1} [11, 12]. This could be theoretically ameliorated by using an effective, direct, and promising strategy, i.e., increasing charge cutoff voltage, which is however precluded by irreversible phase transitions, oxygen loss, and severe side reactions with electrolytes normally [13, 14]. On the other side, the relatively scarce abundance of cobalt on earth would result in possible insufficient supply for LIBs [8, 15]. In this sense, to reduce or even abolish the utilization of Co in the derivatives based on $LiCoO_2$ is imperative, which actually has commenced a couple of years before with several milestones has been mainstream for the next decades (Fig. 1). Co-reduced layered oxides (typically high-nickle $LiNi_{0.8}Co_{0.1}Mn_{0.1}O_2$ (NCM811) [16, 17], $LiNi_{0.33}Co_{0.33}Mn_{0.33}O_2$ (NCM111) [18], $LiNi_{0.5}Co_{0.3}Mn_{0.2}O_2$ (NCM532) [19], and so on), Li-rich and manganese-rich (LMROs) [20–22], high-nickel Li-rich (HNLROs) layered oxides [23, 24], cobalt-free layered $LiNiO_2$ (LNOs) [25, 26], olivine $LiFePO_4$ (LFP) [27, 28], spinel $LiMn_2O_4$ [15, 29], and novel Li-excess cation-disordered rock-salt (DRX) ($Li_{1.3}Mn_{0.4}Nb_{0.3}O_2$, $Li_{1.2}Mn_{0.4}Ti_{0.4}O_2$, $Li_{1.2}Ni_{1/3}Ti_{1/3}Mo_{2/15}O_2$, $Li_4Mn_2O_5$, and $Li_2FeV_{0.5}Ti_{0.5}O_4$) oxides [30, 31] have sequentially emerged and grown rapidly. Some of them have been commercialized or taken as next-generation potential cathode materials owing to their intrinsically high theoretical and/or practical capacities with a cost acceptable [9, 15, 32–34].

Though layered LCOs oxides could deliver potentially high capacity at high voltages such as 4.6 V, their high-voltage stability is still far from satisfactory as a consequence of oxygen loss in the lattice [35, 36], harmful phase transition ($CoO_2 \rightarrow Co_3O_4$) [37, 38], crack formation [14], particle pulverization [13, 39], and serious

Address correspondence to wgchu@nanoctr.cn

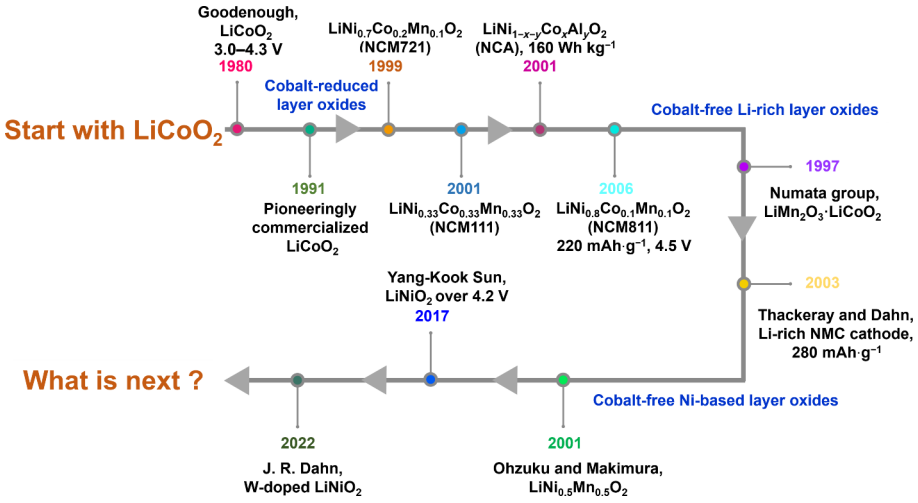

Figure 1 The milestones of layered cathodic materials for LIBs: from Co-containing to Co-free layered oxides. The references of every milestone are shown as follows: Goodenough, J. B. etc., *Mater. Res. Bull.*, 1980, 15, 783–798; Lee, J. Y. etc., *J. Power Sources*, 1999, 81, 416–425; Makimura, Y. etc., *Chem. Lett.*, 2001, 30, 642–651; Macklin, W., *J. Power Sources*, 2001, 97, 733–742; Sun, Y., *J. Power Sources*, 2006, 159, 1328–1333; Numata, K., *Chem. Lett.* 1997, 26, 725–726; Dahn, J. *J. Electrochem. Soc.* 2003, 150, A1637–A1645; Makimura, Y., *Chem Lett.*, 2001, 8, 744–753; Sun, Y., *ACS Energy Lett.*, 2017, 2, 1150–1155; Dahn, J., *Adv. Energy Mater.*, 2022, 12, 2103067–2103075.

interface side reactions [40, 41] normally taking place during cycling. In view of the requirement of 350 Wh·kg^{-1} and 750 Wh·L^{-1} energy density at the cell level for a 500-mile driving range in a single charge of EVs, as established by the U.S. Department of Energy (DOE) and U.S. Advanced Battery Consortium (USABC) [42], Ni-based layered oxides with Ni contents higher than 80% are considered to be competent due to their high specific capacities (250–270 mAh·g^{-1}), acceptable working voltages (3.6–3.8 V versus Li/Li$^+$), and relatively low cost [15, 43, 44]. Nevertheless, high-nickel layered oxides, especially LNOs, have electrochemical instabilities, environmental sensitivity, and much worse mechanical stability, especially at relatively high cut-off voltages (> 4.3 V), due to undesired phase transformations, intergranular and intragranular cracking, and corrosion and dissolution of transition metals after prolonged cycling [45–51]. Thus, a compromise between LCOs and LNOs from the perspectives of chemical constituents and performance led to the emergence of some typical Co-reduced layered oxides such as NCM811 [16, 17] and NCM532 [19]. Further combining Ni-based layered oxides with Li_2MnO_3, Li-rich layered oxides (LROs), especially LMROs, are designed to exhibit both anionic and cationic redox due to their high energy storage capacities [21, 52, 53]. Unfortunately, their formidable voltage hysteresis/decay reduces the energy conversion efficiency of the battery, which is a critical limitation to their commercial application [22, 44, 54]. Increasing nickel content in LMROs can achieve HNLROs, which is an effective and simple way to address the issue of the rapid voltage decay of LMROs, but normally accompanies by reduced capacity and inferior cycling stability [23, 33, 55].

In contrast, commercialized olivine LFPs and spinel $LiMn_2O_4$ show less complicated crystal structures, better cycling stability, and lower cost despite their lower capacities. Both the relatively low capacity (~ 170 mAh·g^{-1}) and voltage plateau (~ 3.3 V) for LFP determine its relatively low energy density, which, along with poor electrical conductivity at low temperatures, would greatly influence large-scale applications in the long run though widely commercialized at present [9]. Spinel $LiMn_2O_4$ may undergo a large volumetric change during cycling since Mn^{3+} is prone to Jahn–Teller distortion, which together with its low capacity also limits its large-scale commercialization [15]. Novel DRX with high energy densities and facile Li transport intrinsically enabled by a percolating network of Li-rich environments (0-TM or 1-TM channels) are the newly emerging cathode family members [30, 31]. DRX is expected to be quite potential in the future, despite possible capacity loss caused by the valence state changes of transition metal (TM) and the increased impedance of Li$^+$ transport as a result of oxygen loss during cycling [30, 31]. Therefore, specific strengths and weaknesses of these cathode materials developed so far would determine how far they would go in practical applications with ever-increasing demand for energy density.

This review will aim to provide a comprehensive overview about the cathode materials from layered $LiCoO_2$ especially at high voltages to Co-reduced /Co-free layered oxides for LIBs with emphasis on performance, problems, and potentials from the perspectives of the challenges of novel structures, surface modification, and heteroatoms dopants. Furthermore, to optimize the performance of full-cells, the accurate selection of anodes materials suitable for different novel cathodes is a key and will be discussed briefly.

2 Layered cobalt-containing oxides cathodes

2.1 Layered high-voltage $LiCoO_2$ cathodes

LCOs with a layered rhombohedral structure (space group $R\bar{3}m$) were discovered by Goodenough in 1980s and firstly commercialized for LIBs by Sony Company in 1991 [13]. Although LCO shows a theoretical specific capacity as high as 274 mAh·g^{-1}, the practical capacities around 175 mAh·g^{-1} for a cutoff voltage of 4.45 V could be normally delivered because of cobalt dissolution and oxygen loss, crack formation/particle pulverization, harmful phase transition (CoO_2 → Co_3O_4), and drastic electrolyte penetration [13, 15, 35, 42]. As a type of milestone cathode materials, a great many studies have been devoted to the improvement of performance and the unveiling of underlying mechanisms, still accompanied by the continuing emergence of novel strategies [15, 32, 56]. Main measures for performance improvement are basically focused on surface modification, heteroatoms-doping, and morphology control [35, 36, 41, 57].

2.1.1 Surface modification

Surface coatings/modifications are generally considered as an attractive and effective strategy for surface stability enhancement of numerous cathode materials. The presence of surface modified

layers or coatings would effectively protect LCOs from the attack from electrolyte via the parasitic reactions between cathode and electrolyte [3].

Conventional metallic cation-based modifications/dopants for LCOs were mostly seen in the past decades [36, 40, 58]. Besides, polyanion anions-dopants could also be introduced, which are expected to suppress oxygen loss at high voltage [39]. Tan X. et al. proposed an *in-situ* trace sulfur-assisted one-pot solid-state approach to successfully synthesize long-term highly stable LCOs even at a cutoff voltage as high as 4.6 V (Fig. 2(a)) [39]. The superior performance arises from simultaneous realization of coating coherent spinel $Li_xCo_2O_4$ shells and the sulfur gradiently

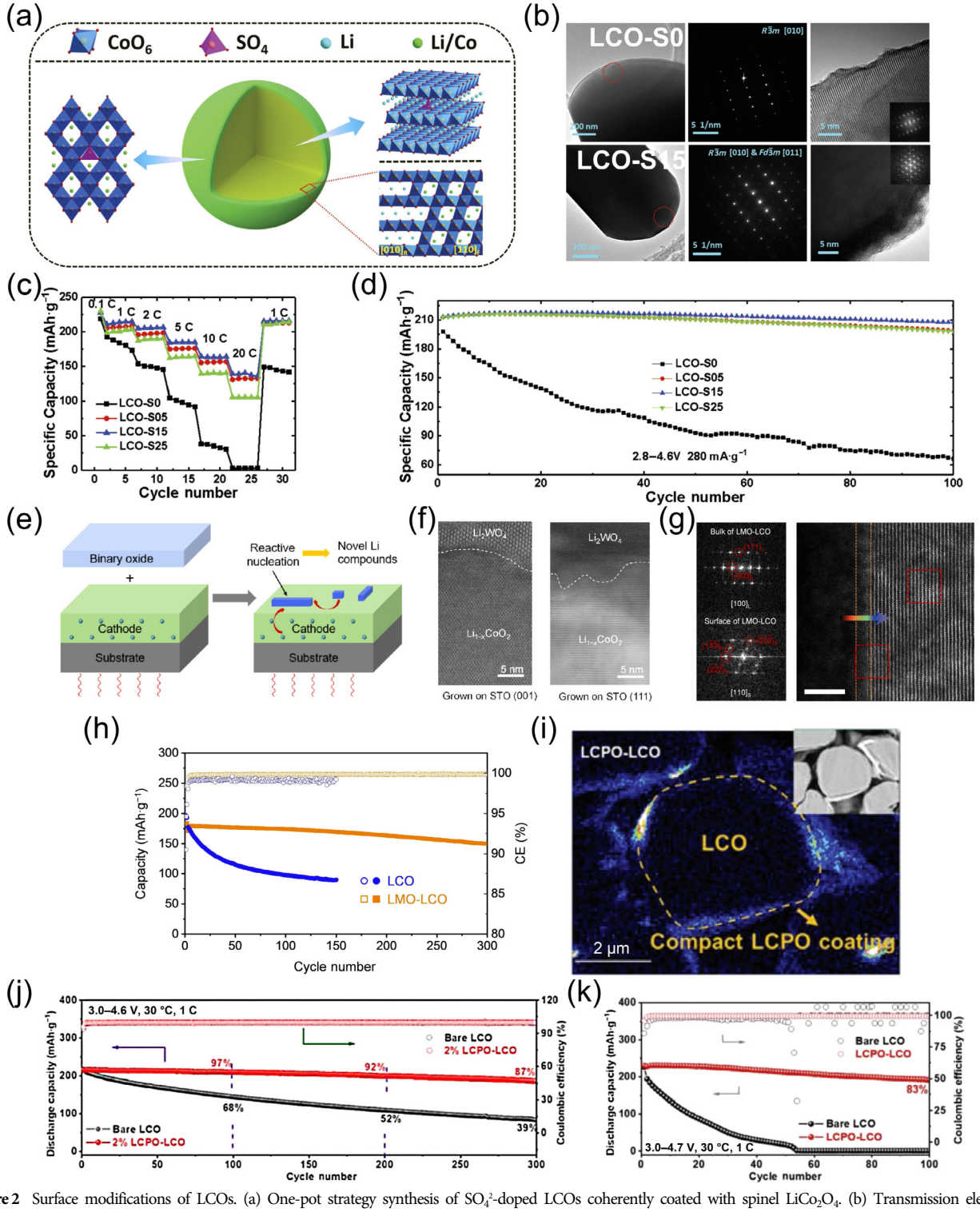

Figure 2 Surface modifications of LCOs. (a) One-pot strategy synthesis of SO_4^{2-}-doped LCOs coherently coated with spinel $LiCo_2O_4$. (b) Transmission electron microscopy (TEM) images, selected area electron diffraction (SAED) patterns, and high-resolution TEM (HRTEM) images of LCO-S0 and LCO-S15, respectively. ((c) and (d)) Rate performances and cycling stabilities of LCO-S0, LCO-S05, LCO-S15, and LCO-S25, respectively. Reproduced with permission from Ref. [39], © Wiley-VCH GmbH 2022. (e) Schematic illustration of epitaxial growth of LCOs and subsequently coated with binary TM oxides. (f) Cross-sectional scanning TEM (STEM) images of $Li_2WO_4/LiCoO_2$ core–shell structures grown on different $SrTiO_3$ (STOs). Reproduced with permission from Ref. [58], © American Chemical Society 2022. (g) High-angle annular dark field (HAADF) image of $Li_4Mn_5O_1$ (LMO)-LCO materials (scale bar: 5 nm). (h) Cycling stability of LMO-LCOs and LCOs under a current density of 135 $mA·g^{-1}$. Reproduced with permission from Ref. [40], © Wiley-VCH GmbH 2022. Mapping image (i) and scanning electron microscopy (SEM) image (inset of (i)) of 2% LCPO coating on LCOs. ((j) and (k)) Cycling performances of bare LCOs and LCPO-LCOs at 1 C, 30 °C within the range of 3.0–4.6 V (j) and 3.0–4.7 V (k). Reproduced with permission from Ref. [36], © Wiley-VCH GmbH 2022.

doped into the near-surface of LCO to form SO_4^{2-} polyanions in terms of *in-situ* gas-solid interface reactions between metal oxides and SO_2 gas generated from sulfur during synthesis (Fig. 2(b)) [39]. At 4.6 V, the LCO thus obtained shows quite high discharge capacities of 232.4, 215.0, and 139.0 mAh·g^{-1} at 0.1, 1, and 20 C (1 C = 280 mA·g^{-1}), respectively, and excellent high-voltage cycling stability with the capacity retentions of 97.4% (89.7%) after 100 (300) cycles at 1 C (Figs. 2(c) and 2(d)) [39]. This approach, different from normal metallic cation surface doping/modification, is quite unique which is facile, low-cost, up-scalable, and easily controllable for performance improvement of other electrode materials as well [39]. However, the low-cost solid state synthesis approach employed here normally is difficult to achieve perfect heterostructures at the surface or sub-surface pertaining to the bulk by prolonging the reacted durations. To address this issue, new synthesis strategies were explored, as revealed by the work of Wang L. et al. [58]. A lithiation-assisted epitaxy approach was proposed to combine different epitaxial interfaces or surfaces, which is favorable for the discovery of novel energy materials but also the construction of a well-defined model system for mechanistic studies of energy storage and conversion processes [58]. A two-step sequence modification was successfully realized via the growth of an epitaxial $LiCoO_2$ cathode layer followed by the deposition of a layer of binary transition metal oxide (Fig. 2(e)) [58]. As a solid-state electrolyte, orientation-controlled Li_2WO_4 could be epitaxially formed by using WO_3 as nuclei to react with Li ions from the underlying cathode on different substrates of STO (001) or STO (111) (Fig. 2(f)) [58]. To enhance the high-voltage cycling stability, Liu J. et al. discovered that LCOs passivated with spinel $Li_4Mn_5O_{12}$ (spinel $Li_4Mn_5O_{12}$-coated LCOs) can exhibit a high specific capacity of 194 mAh·g^{-1} at 0.05 C and a capacity retention of 83% after 300 cycles at 0.5 C as a result of the formation of an anion-rich inner Helmholtz layer after charging (Fig. 2(h)) [40]. Because of normal severe structural and interfacial degradation at the voltages higher than 4.55 V for LCOs, Yang X. et al. proposed to coat LCOs with lattice-matched $LiCoPO_4$ (LCPO) for the enhancement of long-term cycling stability for the cut-off voltage as high as 4.7 V (Fig. 2(i)) [36]. The side reactions between LCO and electrolyte such as O loss/Co dissolution, irreversible phase transition, or intergranular cracking were remarkably alleviated because of the introduction of a lattice-matched LCPO coating [36]. This substantially improved long-term cycling stability at room temperature (30 °C) within 3.0–4.6 V (Fig. 2(j)), and rate performance even for an ultrahigh cut-off voltage of 4.7 V (Fig. 2(k)) [36]. Therefore, relative to the conventional approaches of solid-state surface modifications, the approach of chemical reaction-driven lattice-coherent surface modifications here not only can realize surface coherent coatings, modifications, and/or doping of LCOs with various compounds of appropriate crystalline structures via proper processes but also enables to provide ideal models for in-depth mechanistic studies of electrochemical processes. At the same time, the stable and compact coherent surfaces via surface modifications are normally inert to the electrolyte which usually shows far more positive effects in electrochemical performance compared with the loose and incoherent modifications. Thus, it is natural to conclude that the strategy of chemical reaction-driven lattice-coherent surface modification is expected to play an increasingly important role in performance breakthrough of LCOs at ultrahigh-voltages including significant improvement of both capacity and cycling stability which thus may satisfy the demands of high energy density for LIBs [36].

Therefore, as far as surface modifications, although significant capacity escalation and stability enhancement of LCOs at high voltages, some issues such as non-uniform and non-continuous modifications, coating layer cracking during cycling, and/or high cost due to complicated processes still need to be addressed. Since surface modifications could normally take place at the surface or subsurface layers of a LCOs particle, their performance improvement is reasonably limited as a consequence of most intrinsic properties of a pristine bulk particle still maintained. In this sense, other strategies for performance improvement are still to be developed.

2.1.2 *Heteroatoms doping*

As already mentioned above, surface coatings, modifications, and/or doping are not sufficient for performance enhancement of LCOs. As another type of performance improvement strategy mostly seen, heteroatoms (bulk) doping is expected to be capable of modifying the electronic structure of electrode materials which would probably vary their chemical and physical properties and thus improve electrochemical performance more remarkably compared with surface and/or subsurface modifications only. Technologically, lanthanide (Ln)-doped LCOs with Ln being rare earths such as La, Pr, Nd, Sm, Eu, Gd, Er, and Lu were successfully realized and revealed to display remarkably improved cycling stability [59]. Other electrochemically inactive single- or multi-cation doping such as Zr^{2+}, Mg^{2+}, Al^{3+}, Ba^{2+}, and Ti^{4+} could also enhance the cycling stability effectively, especially at high voltages over 4.45 V [57, 60–62]. One should bear in mind that the replacement of Co in LCOs by proper amount of electrochemically-active Ni could also effectively stabilize the layered structure to enhance the electrochemical performance at 4.6 V. This is quite different from the doping of those electrochemically inactive heteroatoms above because the active Ni^{3+} dopants could be oxidized to higher states during charging and thus may contribute to both capacity escalation and cycling stability with remaining Co^{3+} capable of improving electron conductivity and suppressing cationic mixing [16, 19, 43, 63]. Therefore, the doping of nickel with different quantities into LCOs can be actually taken as a measure to develop a new type of layered oxide cathodes with Co-reduction which will also be discussed in the following.

Usually, the heteroatomic dopants are considered to occupy Li sites or TM sites in LCOs. Jia K. et al. employed $LiNi_{0.5}Mn_{0.3}Co_{0.2}O_2$ as Ni/Mn sources to realize the co-doping of Ni/Mn into LCO by direct mixing followed by heat treatment [19]. The co-doping of Ni/Mn into the Co layer can enhance the Co–O bonding for suppression of oxygen release and harmful phase transformations and thus stabilization of the layered structure during delithiation, which leads to superior electrochemical performance at 4.6 V (Figs. 3(c) and 3(d)) [19]. Clearly, the replacement of the majority of Co by Ni/Mn can enhance the energy density and electronic conductivity of LCO by effectively interacting with Co to vary the properties of LCO greatly. This not only provides an effective route of improving the performance of LCO but also establishes a model platform for the exploration of underlying mechanisms and points out a right direction for cost reduction by decreasing the percentage of Co significantly. Different from the Li-sites occupation, Xia J. et al. doped Ln into LCO by partially replacing Li in the Li sites to enhance the structure stability for the improvement of high-voltage performance via tuning the lattice strains in terms of the lanthanide contraction (Figs. 3(a) and 3(b)) [59]. Huang Y. et al. thought of the dopants of Mg ions as pillars in the Li-slab of LCO to prevent slab sliding in a delithiated state, thereby suppressing unfavorable phase transitions (Figs. 3(e) and 3(f)) [57]. The doping of Mg into the Li site led to a capacity as high as 204 mAh·g^{-1} at 0.2 C, and a capacity retention of 84% at 1.0 C for 100 cycles within a potential window of 3.0–4.6 V (Fig. 3(g)), in

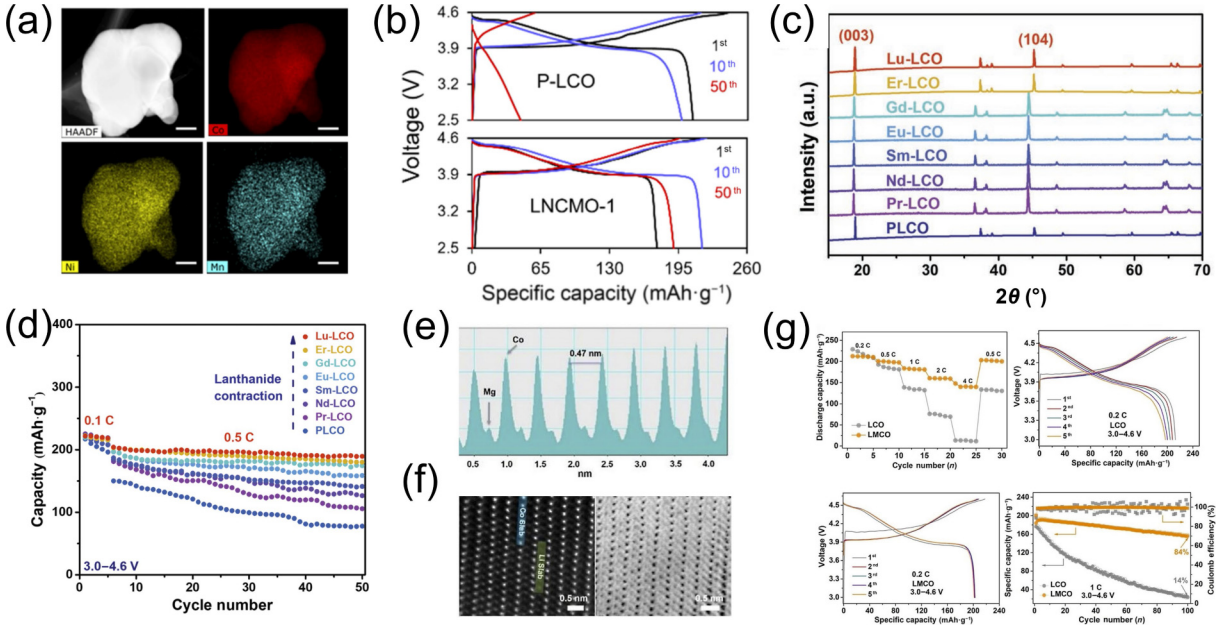

Figure 3 Heteroatom-doped of LCOs. (a) Elemental mappings of an (Ni, Mn)-dope LNCMO particle (scale bars: 500 nm) and (b) comparison of voltage profiles of pristine P-LCO (top) and doping-modified LNCMO-1 (bottom) cycled after different times at 0.5 C within a potential range from 2.5 to 4.6 V. Reproduced with permission from Ref. [19], © American Chemical Society 2022. (c) X-ray diffraction (XRD) patterns of Ln-doped LCOs and pristine LCOs and (d) their cycling performance within a potential range of 3.0–4.6 V. Reproduced with permission from Ref. [59], © Wiley-VCH GmbH 2022. (e) Intensity plot corresponding to (f) the lattice fringes shown by HADDF and STEM-ABF images of LMCOs. (g) Comparison of rate capability, charge/discharge profiles at 0.2 C, and cycling performance at 1 C for pristine LCOs and modified LMCOs within a potential range of 3.0–4.6 V. Reproduced with permission from Ref. [57], © Wiley-VCH GmbH 2020.

sharp contrast with only 14% for pristine LCO [57]. The much improved performance could be ascribed to the pillaring effect of Mg which can effectively stabilize the structure of LCO to prevent the formation of cathode-electrolyte interphase (CEI) and phase transformation in the surface and sub-surface regions [57]. The Mg-pillar in Li sites instead of traditional in Co sites would stabilize the bulk structure and consequently enhance the cycling performance even at a high voltage (4.6 V), which is a novel viewpoint for structure-engineering.

It is clear that the doping replacement of Co in the transition metal site and of Li in the Li site by alien elements in the lattice of LCO can both enhance the electrochemical performance significantly. However, their underlying mechanisms for improving the performance may be totally different, even for different alien elements with different valence states and/or electrochemical activities. Furthermore, different doping strategies even for the identical alien elements would also produce totally different effectiveness of performance enhancement since their thermodynamics and/or kinetics may differ as well to lead to the formation of modified LCOs with quite different microstructures, morphologies, dimensions, defects, and even crystallinity. Therefore, selection of both alien elements and preparation strategies and their processes are quite critical for electrochemical performance improvement.

2.2 Cobalt-reduced ternary cathode materials

It has been demonstrated that both surface coating/modifications and heteroatom doping can enhance the performance of LCOs by different degrees with the Co in LCOs as both electrochemically active centers and electrically conductive promoters. However, the high cost and scarcity of cobalt resources would undoubtedly restrict large-scale production and applications of LCOs. Therefore, the decrease of Co portion in LCOs is taken as a goal to develop Co-reduced layered oxides, such as those representatives of NCM111, NCM532, $LiNi_{0.6}Co_{0.2}Mn_{0.2}O_2$ (NCM622), and NCM811 [9, 15, 32]. However, these Co-reduced and nickel-increased layered oxides also suffer from microstructural and electrochemical instability caused by parasitic phase transformations, stress-driven cracking, and corrosion and dissolution of transition metals after prolonged cycling [45, 46].

Similar to LCOs, surface coatings/modifications and alien element doping can also be employed for performance enhancement of the Co-reduced layered oxides. Zou L. et al. coated NCM532 with 1 wt.% graphite layer via a heat treatment process, which revealed a discharge capacity of 132.96 $mAh·g^{-1}$ with a capacity retention of 91.51% after 40 cycles at 1 C compared with the bare NCM532 [66]. Wang J. et al. successfully realized a compact bilayer coating composed of a cyclized polyacrylonitrile outer layer and a rock-salt bridge-like inner layer by simply mixing and heating polyacrylonitrile and NCM811 in a proper ratio via a thermochemical cyclization strategy (Fig. 4(a)) [16]. The compact bilayer coating can lead to a high reversible capacity of 183 $mAh·g^{-1}$ and a high capacity retention of 83% after 300 cycles at 1 C for NCM811 (Fig. 4(b)) [16]. This facile and scalable surface engineering strategy makes Ni-rich cathodes potentially viable for commercialization for high-energy Li-ion batteries [16]. Jamil S. et al. achieved a Li/Ni antisite-induced disordered passivation layer onto the surface of $LiNi_{0.94}Co_{0.03}Mn_{0.03}O_2$ by Ta and Al co-doping (Fig. 4(c)) [43]. The ultrathin disordered layer is helpful for improving the electronic and ionic conduction, stabilizing lattice oxygen, and alleviating the Ni/Co dissolution and irreversible phase transition [43]. Therefore, superior cycling stability (retention of 90.09% at 0.5 C between 2.7–4.3 V), excellent rate capability, and improved Li^+ diffusion were achieved (Figs. 4(d) and 4(e)) [43].

The work above reveals that regular surface modification can enhance the performance of Ni-rich NCM, but is accompanied by an intrinsic and inevitable anisotropic volume variation because of the insertion and extraction of interlaminal ions upon charge/discharge. To suppress the volume change to stabilize NCM oxides, some novel structures or morphologies like perovskite phase rivet and high-entropy oxides have also been proposed and realized [64, 65, 67]. Tan X. et al. introduced a spinel-like mortise-tenon (MT) architecture into the structure of

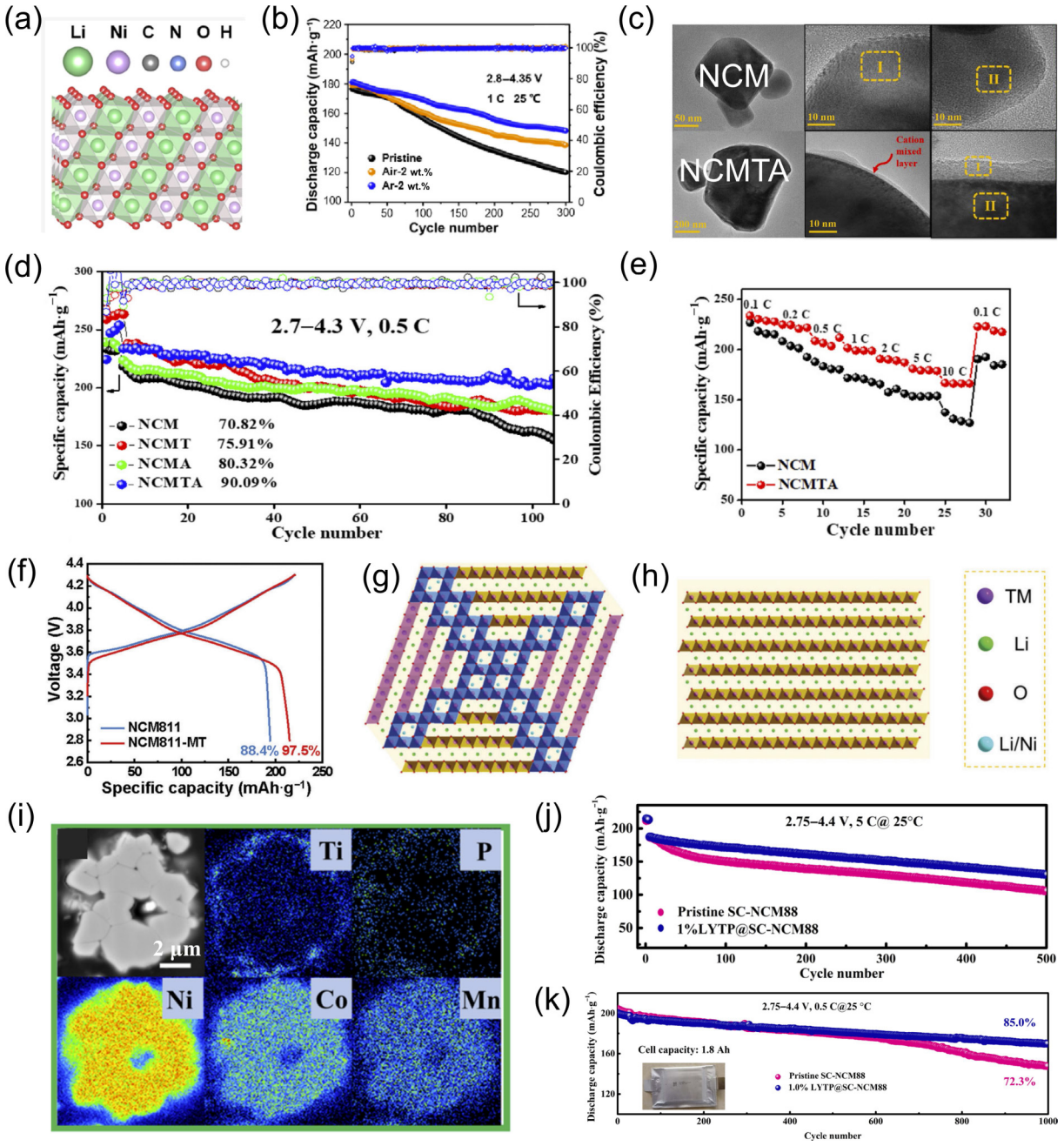

Figure 4 (a) Computational models of super cells of NCM811 cathodes. (b) Cycling performance of pristine NCM811 and two different NCM811 samples modified with polyacrylonitrile at 1 C within a potential range of 2.8–4.36 V. Reproduced with permission from Ref. [16], © American Chemical Society 2022. (c) TEM images of $LiNi_{0.94}Co_{0.03}Mn_{0.03}O_2$ (NCM) and Al/Ta co-doped NCM (NCMTA). (d) Cycling performance of NCM, Al-doped $LiNi_{0.94}Co_{0.03}Mn_{0.03}O_2$ (NCMA), Ta-doped $LiNi_{0.94}Co_{0.03}Mn_{0.03}O_2$ (NCMT), and NCMTA. (e) Rate capabilities of NCM and NCMTA. Reproduced with permission from Ref. [43], © Elsevier B.V. 2021. (f) Initial charge/discharge profiles at 0.1 C for pristine NCM811 and NCM811-MT. ((g) and (h)) Schematic of particles with coupled MT structures (g) and a plain layered structure (h). Reproduced with permission from Ref. [64], © Wiley-VCH GmbH 2023. (i) Cross-sectional electron-probe micro-analysis (EPMA) of 1% LYTP@SC-NCM88 with the corresponding selected area LYTP mapping results of Ni, Co, Mn, Ti, and P elements. Cycling tests of half cells (j) and pouch cells (k) of SC-NCM88 and 1% LYTP@SC-NCM88. Reproduced with permission from Ref. [65], © Fan, X. M. et al. 2021.

NCM811 (NCM811-MT) to achieve a discharge capacity of 215 $mAh·g^{-1}$ and an initial coulomb efficiency (ICE) of 97.5% at 0.1 C, and a capacity retention of 82.2% after 1200 cycles at 1 C (Fig. 4(e)) via incorporating lithium sulfate during synthesis [64]. The MT structure shown in Figs. 4(f) and 4(g) as a novel strain-retardant can effectively suppress the volume variations and provide a high way for fast lithium-ion transport as well [64]. With the architectural MT joints as perfect connection, the layers of NCM811 are wedged into each other through the jagged ends at the spinel-like MT zones [64]. As a consequence, the MT structure can effectively regulate the detrimental anisotropic volume change to stabilize the structure and achieve a high capacity as well.

Furthermore, Fan X. et al. reported a strategy of *in-situ* constructing an $Li_{1.4}Y_{0.4}Ti_{1.6}(PO_4)_3$ (LYTP) ion/electron conductive network at the surface of single-crystal $LiNi_{0.88}Co_{0.09}Mn_{0.03}O_2$ (SC-NCM88) particles to form a uniform and conformal three-dimensional (3D) conductive network connecting the active particles (Fig. 4(h)) [65]. The LYTP-modified SC-NCM88 cathodes display a capacity of 130 $mAh·g^{-1}$ after 500 cycles at 5 C within a voltage window of 2.75–4.4 V at 25 °C (Fig. 4(i)), and their pouch cells paired with graphite anodes present a capacity retention of 85% after 1000 cycles at 0.5 C (Fig. 4(j)) [65]. The enhanced cycling stability of NCM-based cathodes can be attributed to the crosslink network structure which mitigates the mechanical instability by preventing the detrimental phase transformation [65].

For the representative type of Co-reduced layered oxides above, surface modifications via regular or unusual approaches have been demonstrated to be capable of enhancing performance significantly. Generally speaking, these modification strategies can normally be applied for large-scale production with acceptable cost though different mechanisms may take effect in performance improvement. As regards heteroatoms-doping, these particular types of layered oxides derived from LCOs with well-defined stoichiometric design may be just permitted for slight variations in chemical constituents and their relative portions for performance enhancement [3, 38, 68]. Therefore, surface modifications may be more preferred for these NCM111, NCM532, NCM622, and NCM811 cathodes from the perspective of practical applications, i.e., cost and performance.

3 Cobalt-free Li-rich layered oxides

As discussed above, the introduction of nickel and/or other elements into the transition metal lattice site of layered LCOs can improve the performance and decrease the content of cobalt for cost reduction as well. In contrast, another representative type of layered structure oxides, Li-rich layered oxides (LROs) composed of $LiCoO_2$ $R\bar{3}m$ and Li_2MnO_3 $C2/m$ phase components, was pioneeringly prepared by Numata group in 1997 [71]. LROs could be described as $xLi_2MnO_3{\cdot}(1-x)$ $LiTMO_2$ ($0 < x < 1$) (TM = Ni, Co, Mn, etc.) with $LiTMO_2$ and Li_2MnO_3 as the hexagonal and monoclinic layered structures, respectively (Figs. 5(a) and 5(b)) [20, 33, 52]. As pointed out above, in reality, a consensus has been reached that LROs are composed of atomically integrated

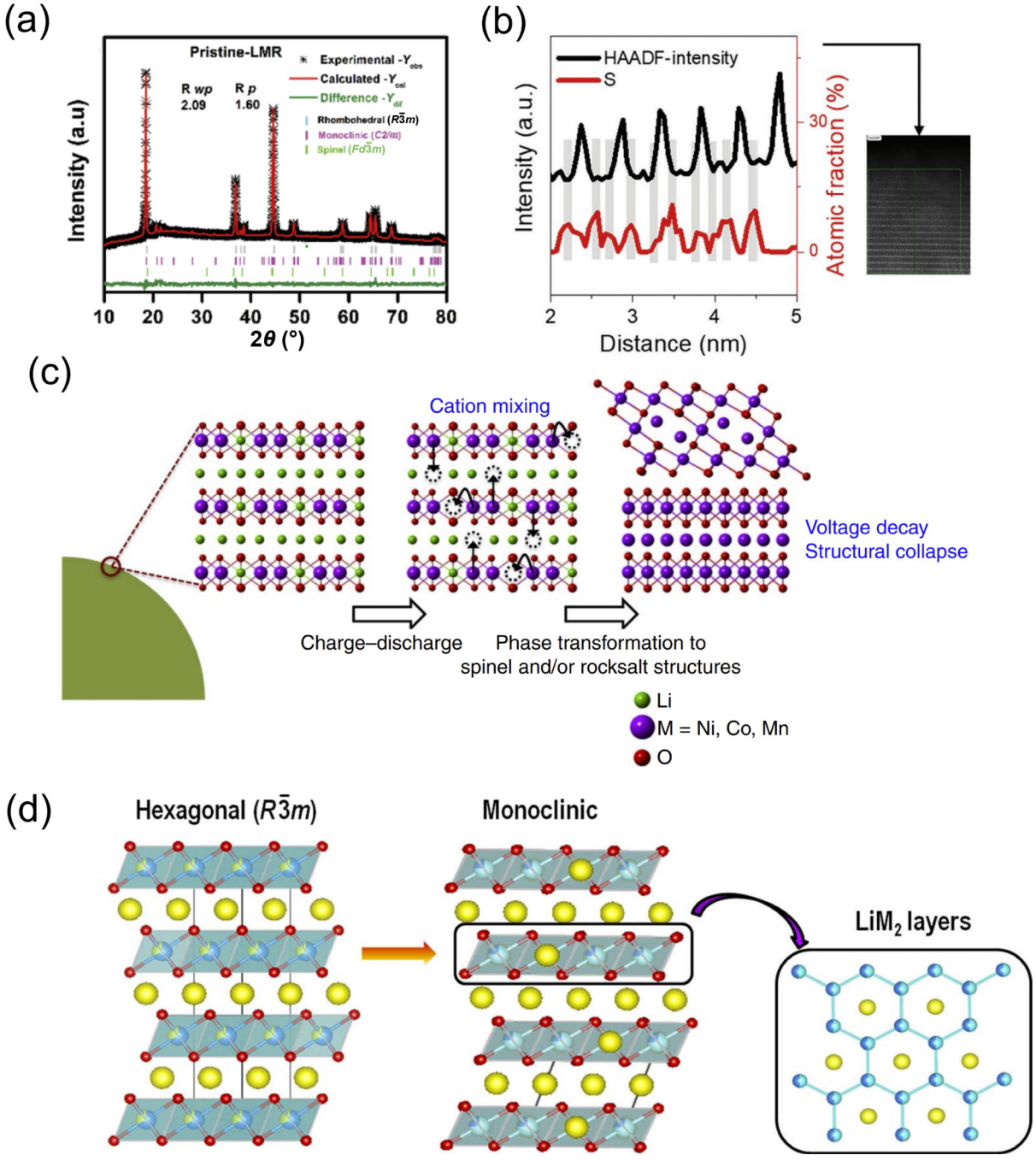

Figure 5 The structure of LMROs. (a) XRD pattern of pristine LMROs. Reproduced with permission from Ref. [53], © He, W. et al. 2019. (b) Energy dispersive spectroscopy (EDS) line scans and HAADF-STEM image of S-LLOs. Reproduced with permission from Ref. [21], © Wiley-VCH GmbH 2022. (c) Crystal structures near the surfaces of Li-rich layered oxides during the charge–discharge process and the structure changes which caused the voltage decay. Reproduced with permission from Ref. [69], © Kim, S. et al. 2016. (d) Structural representation of O3-type the layered oxides. Reproduced with permission from Ref. [70], © The Electrochemical Society 2015.

Li_2MnO_3 and $LiTMO_2$ phases with the octahedral sites of LiO_6 and TMO_6 occupied by Li and TM atoms, respectively, showing an O3-type layered structure rather than a continuous and uniform single phase [70, 72]. The complication of crystal structure also brings about the controversy that LROs are a solid solution composed of Li_2MnO_3 and $LiTMO_2$ layered components with the arrangement of oxygen in a hexagonal close packing array and the alternative arrangement of Li layers and TM/Li mixed layers (Fig. 5(c)) [16, 73–75]. Here, two kinds of LROs, i.e., LMROs and HNLROs, are discussed in detail including their progress, peculiarities, and modifications.

3.1 LMROs

LMROs are considered the most promising cathode candidates for next-generation high-energy lithium-ion batteries because of their high specific capacity [20, 21]. The theoretical capacity of LMROs can reach up to 460 $mAh·g^{-1}$ with a high energy density (> 1000 $Wh·kg^{-1}$) which is much higher than that of the general layered oxides cathodes, say, LCOs, etc., because of the special Li-rich structure with extra oxygen for electronic compensation during charge/discharge [73, 76, 77]. The ratios of the Li_2MnO_3- and $LiTMO_2$-like components in LMROs would have a significant influence on their properties and further electrochemical performance. Therefore, the species of TM in and the portion of the $LiTMO_2$-like phase, along with element doping, surface modifications, and morphological design and control, are normally explored extensively for performance improvement and underlying mechanisms [74–76].

$(1-x)Li_2MnO_3$-$xLiTMO_2$ (TM refers to Co, Fe, Ni, Cr, Nb, Ti, Mo, and Al) is a typical and well-accepted formula of LMROs, which displays high capacities (> 280 $mAh·g^{-1}$) [73, 75]. In the TM/Li mixed layer, lithium and TM atoms are arranged to form a super lattice structure in an ordering way [22, 78]. The reaction of LMROs of the initial charge process is regarded as follows

$$LiTMO_2 \leftrightarrow Li_{1-x}TMO_2 + xLi^+ + xe^- \quad (2.0-4.5\ V) \tag{1}$$

$$Li_2MnO_3 \rightarrow MnO_2 + Li_2O \quad (4.5-4.8\ V) \tag{2}$$

or

$$Li_2MnO_3 \leftrightarrow Li_xMO_2 + (2-x)Li^+ + \frac{1}{2}O_2 + (2-x)e^- \quad (4.5-4.8\ V) \tag{3}$$

Although LMROs could show quite high capacities, LMROs normally suffer from severe voltage decay originating from TM migration and structural transitions from a layered to spinel and/or rock salt phase, low ICE, and poor rate capability upon cycling caused by oxygen release (Fig. 5(d)) [24, 75, 77, 79, 80]. Therefore, from a viewpoint of practical applications, these salient issues have to be addressed via proper strategies as stated above [23]. In past decades, some of them, along with design of chemical constituents of LMROs, have been well demonstrated to show superior cycling performance in terms of different mechanisms [9, 21, 77, 81].

Shao Q. et al. achieved the cycling stability of $Li_{1.2}Ni_{0.13}Co_{0.13}Mn_{0.54}O_2$ with a typical structure of LMROs substantially enhanced with the assistance of the S^{2-}/SO_3^{2-} redox couple by adding $Na_2S·9H_2O$ into the cathodic slurry and followed by doctor-blade casting onto aluminum foil (Fig. 6(a)), say, a retention of 100% after 700 cycles at 1 C (Figs. 6(a) and 6(b)) [75]. The surface peroxide ions (O_2^{2-}) are readily chemically reduced back to immobile O^{2-} by S^{2-} during charging, accompanied by the

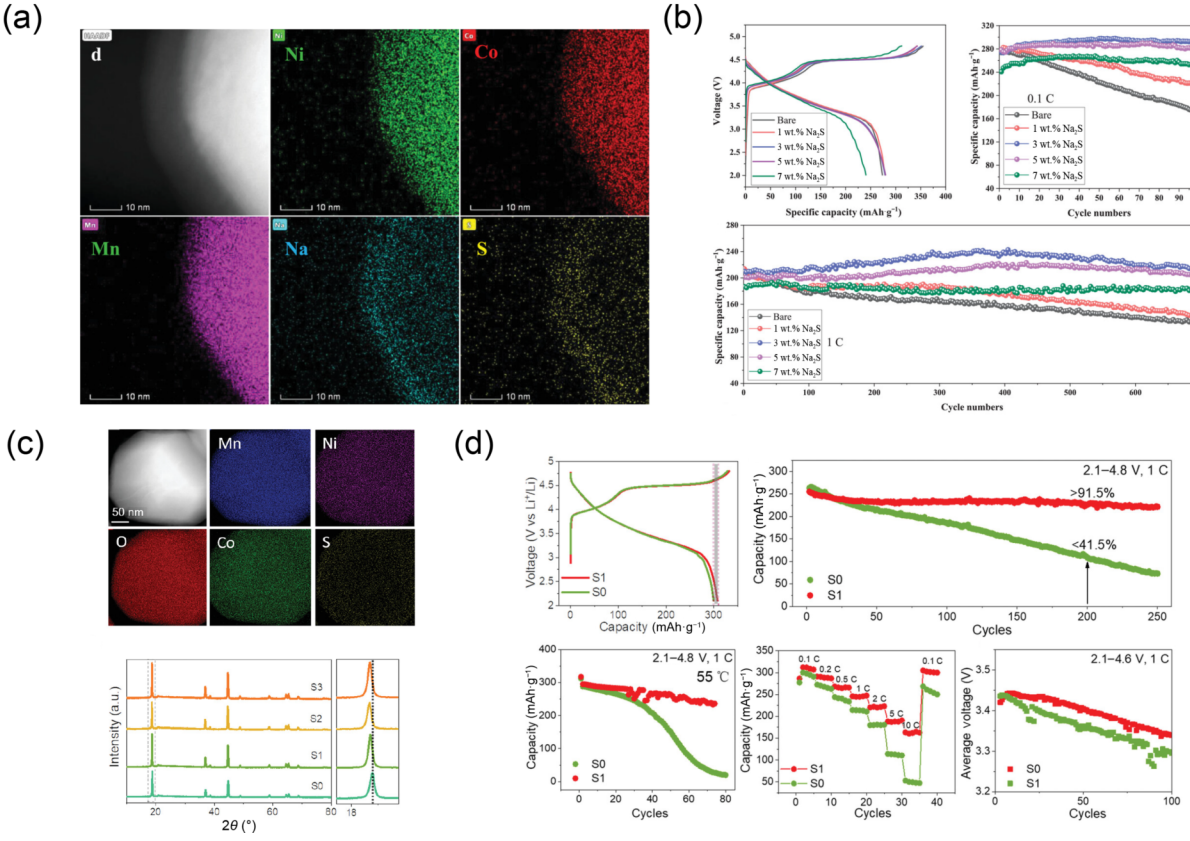

Figure 6 (a) HADDF-STEM images and element mappings of a typical LMRO structure $Li_{1.2}Ni_{0.13}Co_{0.13}Mn_{0.54}O_2$ with 3 wt.% Na_2S. (b) Electrochemical performance of $Li_{1.2}Ni_{0.13}Co_{0.13}Mn_{0.54}O_2$ with S^{2-}/SO_3^{2-} redox couples of different quantities , including initial charge/discharge curves and cycling performance at 20 $mA·g^{-1}$ within a range of 2.0–4.8 V and cycling stability at 200 $mA·g^{-1}$. Reproduced with permission from Ref. [75], © Wiley-VCH GmbH 2022. (c) EDS mappings and XRD patterns of S-LLO. (d) Electrochemical performance of pristine LLO and S-LLO, including the first chargedischarge curves (0.1 C, 2.1–4.8 V), cycling performance at 1 C, cycling performance at 80 °C, rate capabilities, and average voltage evolution. Reproduced with permission from Ref. [21], © Wiley-VCH GmbH 2022.

formation of SO_3^{2-}, which plays a critical role in stabilizing the oxygen lattice and eventually inhibiting the release of oxygen [75]. Another important sulfurization process for $Li_{1.2}Ni_{0.13}Co_{0.13}Mn_{0.54}O_2$ (S-LLOs) was proposed by Zhang K. et al., in which sulfur anions could be incorporated into the oxygen lattice sites and form polyanions at the surface (Fig. 6(c)) [21]. Density functional theory (DFT) calculations also confirmed the contribution of S polyanions in the interior lattice and/or at the surface which would participate in the redox processes of LMROs (denoted as S-LLO) [21]. S polyanions at the surface formed a protection layer for interfacial stability, and those in the lattice promoted the structural stability by mitigating undesired oxygen redox [21]. The as-prepared S-LLO delivered a high discharge capacity of 307.8 mAh·g^{-1} and an outstanding capacity retention of 91.5% after 200 cycles, along with excellent voltage stability, rate capability, and thermostability (Fig. 6(d)) [21]. Liu Q. et al. reported that $0.5Li_2MnO_3{\cdot}0.5LiMn_{0.8}Ni_{0.1}Co_{0.1}O_2$ (Fig. 7(a)) could be successfully prepared by using sol-gel (SLC), sucrose-chelating sol-gel (SLS), and oxalate co-precipitation (OCP) assisted methods [73]. The discharge specific capacities are 261.6 and 138 mAh·g^{-1} at 0.05 and 5 C (Fig. 7(b)), respectively, with a voltage decay of only 210 mV and a capacity retention of 94.2% after 100 cycles at 1 C (Figs. 7(c) and 7(d)) [73]. Figure 7(e) displays that the corrosion of $Li_{1.2}Ni_{0.13}Co_{0.13}Mn_{0.54}O_2$ by the electrolyte was effectively suppressed by doping Na^+ to generate abundant stacking faults using sodium dodecyl sulfate as surfactant [82]. The doped Na^+, which is verified by both Raman spectroscopy and HRTEM images, is uniformly distributed in the lattice of particle instead of just segregation or coating on the surface, as shown in Figs. 7(f)–7(h) [82]. The Na^+-doped LMROs show a high discharge specific capacity of 221.5 mAh·g^{-1} at 5 C and a capacity retention as high as 85.7% after 500 cycles, far better than 64.8% for the pristine-LMROs (Fig. 7(i)) [82]. Luo D. et al. also improved greatly the voltage and capacity stability of LMROs with a capacity retention of 85% after 500 cycles at 1 C and a voltage decay rate of only 0.72 mV per cycle from 30th to 500th cycle through Ti-based modifications (Figs. 7(j)–7(l)) [74]. This work proves that Ti-based modifications can enhance both the voltage and capacity stability which would undoubtedly promote the practical applications of LMROs cathodes in the near future [74].

It has been well revealed that the modifications from heteroatom doping via a small quantity to element substitution by a large quantity can improve both the structural stability and capacity of LMROs [78, 81]. Bruce et al. reported the effective enhancement of structure stability of LMROs by tuning the contents of Mn, Ni, and Co to suppress oxygen loss, as shown in Figs. 8(a)–8(c) [78]. LMROs with three different substitution manners such as $Li_{1.2}Ni_{0.2}Mn_{0.6}O_2$ (LNMO), $Li_{1.2}Co_{0.4}Mn_{0.4}O_2$ (LMCO), and $Li_{1.2}Ni_{0.13}Mn_{0.54}Co_{0.13}O_2$ (LNMCO) were revealed to have different behaviors and electrochemical performances [78, 81]. The Ni-substituted Li_2MnO_3 provides surface protection by forming a relatively thick Ni-rich/Li-poor rock-salt shell, which can impede oxygen evolution from lattice oxygen. In contrast, the Co substitution plays a less critical role in suppressing oxygen loss relative to the Ni-substituted or Ni/Co co-substituted which however can escalate effectively the capacity of LMROs [78]. Beyond the Ni and Co substitutions, Cr was also employed as an effective substitution element to form $Li_{1.2}Cr_{0.4}Mn_{0.4}O_2$ (L-LCMO) with the remarkable mitigation of voltage hysteresis and the superior reversibility of the Cr^{3+}/Cr^{6+} redox couple [81]. $Li_{1.2}Cr_{0.4}Mn_{0.4}O_2$ with partial cation disorder (PD-LCMO) shows a high reversible capacity of > 200 mAh·g^{-1} for 100 cycles at 100 mA·g^{-1} due to the inhibition of Cr collective migration (Figs. 8(d)–8(f)) [81].

Except for element dopings and/or substitutions above, some surface modification strategies were also employed to prevent direct contact between LMROs and electrolyte against being attacked by the electrolyte and suppress irreversible phase

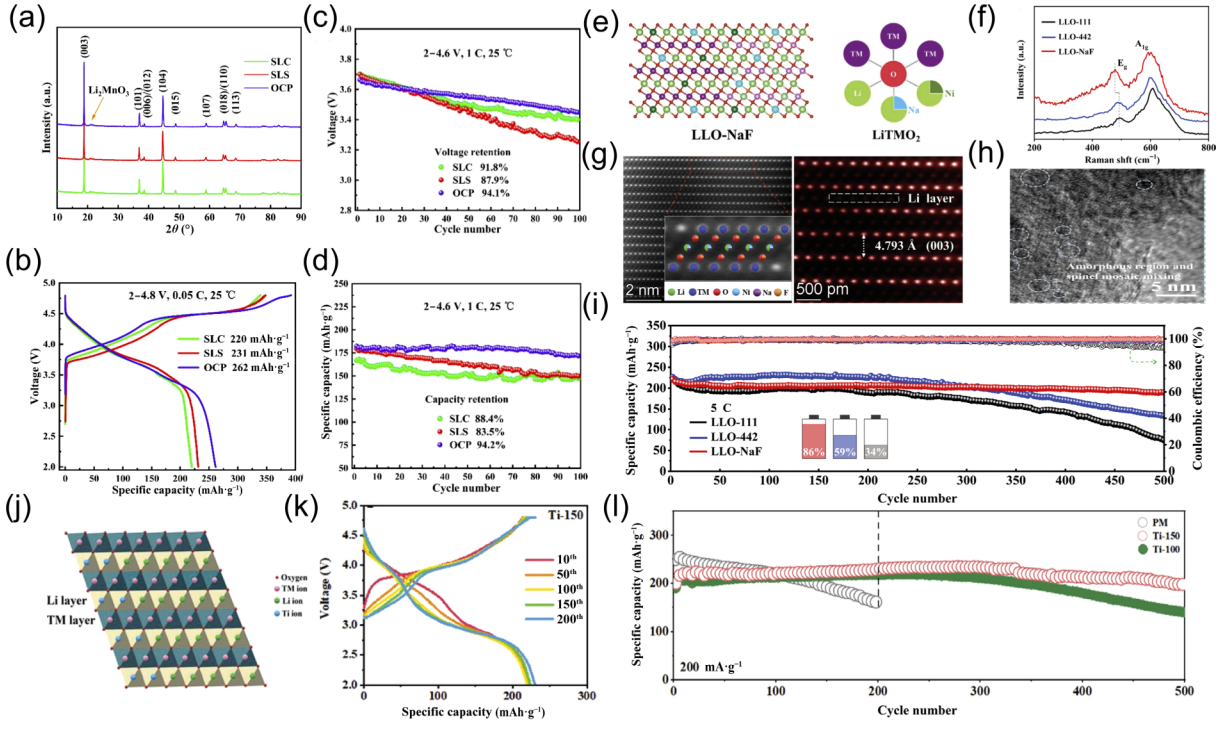

Figure 7 (a) XRD patterns, (b) initial charge/discharge curves, and (c) voltage and (d) specific against cycling for $0.5Li_2MnO_3{\cdot}0.5LiMn_{0.8}Ni_{0.1}Co_{0.1}O_2$ with SLC, SLS, and OCP methods. Reproduced with permission from Ref. [73], © Liu, Q. M. et al. 2021. (e) Schematic illustrations of local atomic coordination around O and TM. (f) Raman spectra. (g) Images along the [010] direction of rhombohedral $LiTMO_2$ ($R\bar{3}m$) for Na^+-doped LMROs. (h) The distribution of Na^+. (i) Cycling performances and corresponding Coulombic efficiencies at 5 C (activated at 0.2 C for the first cycle). Reproduced with permission from Ref. [80], © Wiley-VCH GmbH 2021. (j) Schematic illustration, (k) charge/discharge curves, and (l) cycling stability of modified LMROs based on Ti. Reproduced with permission from Ref. [74], © Wiley-VCH GmbH 2021.

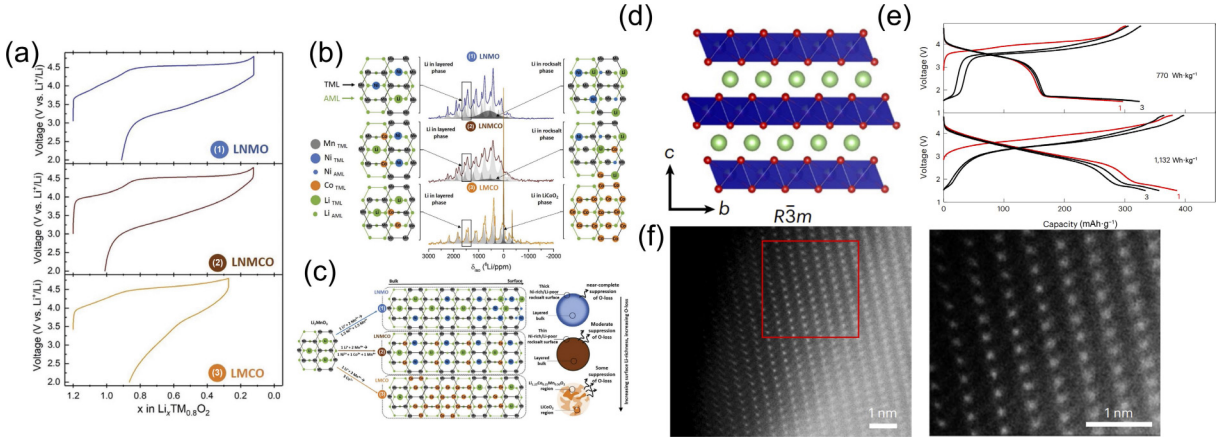

Figure 8 (a) First galvanostatic cycle of LNMO (blue), LNMCO (brown), and LMCO (orange) at 50 mA·g^{-1}. (b) ^{6}Li MAS NMR spectra of (1) LNMO, (2) LNMCO, and (3) LMCO with their corresponding deconvolutions showing the different phase segregation. (c) Schematic representation of local cation distributions in the TM layer in these oxides. Reproduced with permission from Ref. [78], © Boivin, E. et al. 2020. (d) Crystal structures of L-LCMO. (e) Voltage profiles of L-LCMO (top) and PD-LCMO (bottom) at 20 mA·g^{-1} within a voltage window of 4.8–1.5 V for the first 3 cycles at room temperature. (f) HR-HADDF-STEM images of L-LCMO. Reproduced with permission from Ref. [81], © Huang, J. P. et al. 2023.

transformations as much as possible for improvement of rate capability and long-cycle stability [16, 44, 70]. Ding X. et al. reported the enhanced performance of Li-rich oxide LLO using a facile NaF surface modification approach (Fig. 9(a)) [82]. The coating layer of LLOs, which can be observed by a TEM image, consists of a gradient $Na_{1-x}Li_xF$ and $Li_{1.2-x}Na_xNi_{0.13}Co_{0.13}Mn_{0.54}O_2$ bilayer via a Li^+/Na^+ exchange reaction, as shown in Fig. 9(b) [82]. The LLO displays markedly improved cycle life and rate capability as well as suppressed voltage decay, say, a capacity retention of 85% for 1000 cycles at 10 C and a voltage decay of only 2.1 mV per cycle at 0.5 C (Fig. 9(c)) [82]. Furthermore, the N-doped carbon was coated at the surface of $Li_{1.2}Mn_{0.6}Ni_{0.2}O_2$ (LRMNO) via the pyrolysis of urea, which can consequently enhance the voltage and capacity stability of LRMNO (Fig. 9(d)) [22]. Oxygen vacancy and spinel phase integration can suppress irreversible O_2 release and promote lithium ion diffusion, while the N-doped carbon nanolayer mitigates the corrosion of electrolyte with excellent conductivity [22]. The rate capacity of LRMNO retention after 500 cycles at 1 C is 89.9% with a voltage fading rate as low as 1.09 mV per cycle (Fig. 9(e)) [22]. This three-in-one surface treatment strategy can effectively suppress the voltage decay and capacity fading of LLOs which renders it possible to be practically applied [22].

The voltage decay is a key issue for pristine LMROs, as stated. By alien doping, element substitutions, and/or surface modifications, this issue could be addressed by different degrees. However, the degradation mechanisms and solid-state-phase-formed behaviors of LMROs still need to be unveiled. Conventionally, the formation of Li_2O [83], the localization of O 2p electron holes [84], and/or layered-to-spinel phase transitions were proposed for explaining the degradation mechanisms. Recently, a novel viewpoint about the voltage-decay was presented by Hua W et al. [85]. The results based on $Li[Li_{0.2}Ni_{0.2}Mn_{0.6}]O_2$ revealed that the cubic spinel phase (space group $Fd\bar{3}m$) is thermodynamically stable for very low Li concentrations ($0.00 \le x < \sim 0.40$) [85]. The increase of Li content ($\sim 0.04 \le x < \sim 1.2$) would lead to the presence of a triphases-coexistent region, *i.e.*, Li-containing spinel ($Fd\bar{3}m$), Li-containing rock-salt-type ($Fm\bar{3}m$), and Li-rich layered phase ($C2/m$) [85]. Higher portions of lithium ions ($\sim 1.2 < x < \sim 1.52$) would stabilize the monoclinic layered phase ($C2/m$) with a formula of $Li[Li_{0.2+x}(Ni_{0.2}Mn_{0.6})_{1-1.25x}]O_2$ [85]. This study presents unique and new standpoints about the interplay of lithium and oxygen during lithium insertion/extraction which would promote the discovery of novel alkali-rich transition-metal oxides with enhanced electrochemical performance for energy storage applications. Also, *in-situ* high-temperature XRD (HT-XRD) was adopted to reveal that Li species could react with CO_2 to form Li_2CO_3 at high temperatures (100–700 °C) in air which play a peculiar role in the formation of intermediates during the synthesis of Li-rich layered $Li[Li_{0.2}Ni_{0.2}Mn_{0.6}]O_2$ ($C2/m$) [86]. The Li_2CO_3 induced a transformation from the rhombohedral structure ($R\bar{3}c$) to the fully disordered Li-containing rock-salt-type $[Li_xTM_{1-x}]O$ ($0 < x < 0.5$) ($Fm\bar{3}m$) and finally to the monoclinic layered LMROs ($C2/m$) phase as Li/O ions were incorporated upon annealing [86]. These valuable and new findings can provide a robust guidance for the large-scale commercial production of layered LMROs electrodes.

It is shown that a lot of studies about LMROs are focused on the design and tailoring of chemical constituents, followed by surface modifications/coatings, dopings of minute elements, and even element substitutions in large quantity for the discovery of novel oxides, performance improvement, and underlying mechanisms. The design of chemical constituents along with numerous synthesis and modification approaches proposed has led to the discovery of various types of layered oxides with different properties and thus electrochemical performance. All of this partially or fully addressed some critical issues intrinsic to LMROs, which would push their practical applications forward greatly and thus enable LMROs to be one of competing next-generation candidate cathode materials. Of course, with the electrochemical performance to satisfy the demands of applications, safety is the most critical and common issue, as required for other electrode materials. Therefore, safety improvement via stabilizing the structure and other strategies would be another indispensable exploration field for LMROs.

3.2 HNLROs

Although LMROs can be taken as potential cathode materials from the perspectives of both chemical constituents and intrinsic performance, LMROs have not yet gone into commercialization since relatively low ICE, poor rate capability, and voltage decay upon cycling couldn't be well addressed [23, 24, 33, 43, 77]. It has been demonstrated that the increase of Ni content could effectively improve the voltage stability upon cycling as a result of the decrease of layered Li_2MnO_3 component content and the effective suppression of lattice oxygen evolution [32, 33, 87]. Furthermore, Ni ions tend to reversibly migrate among the TM layers during the lithiation–delithiation processes, which can suppress the formation of a spinel phase to improve the cycle stability [43, 75, 79]. Despite the superior electrochemical

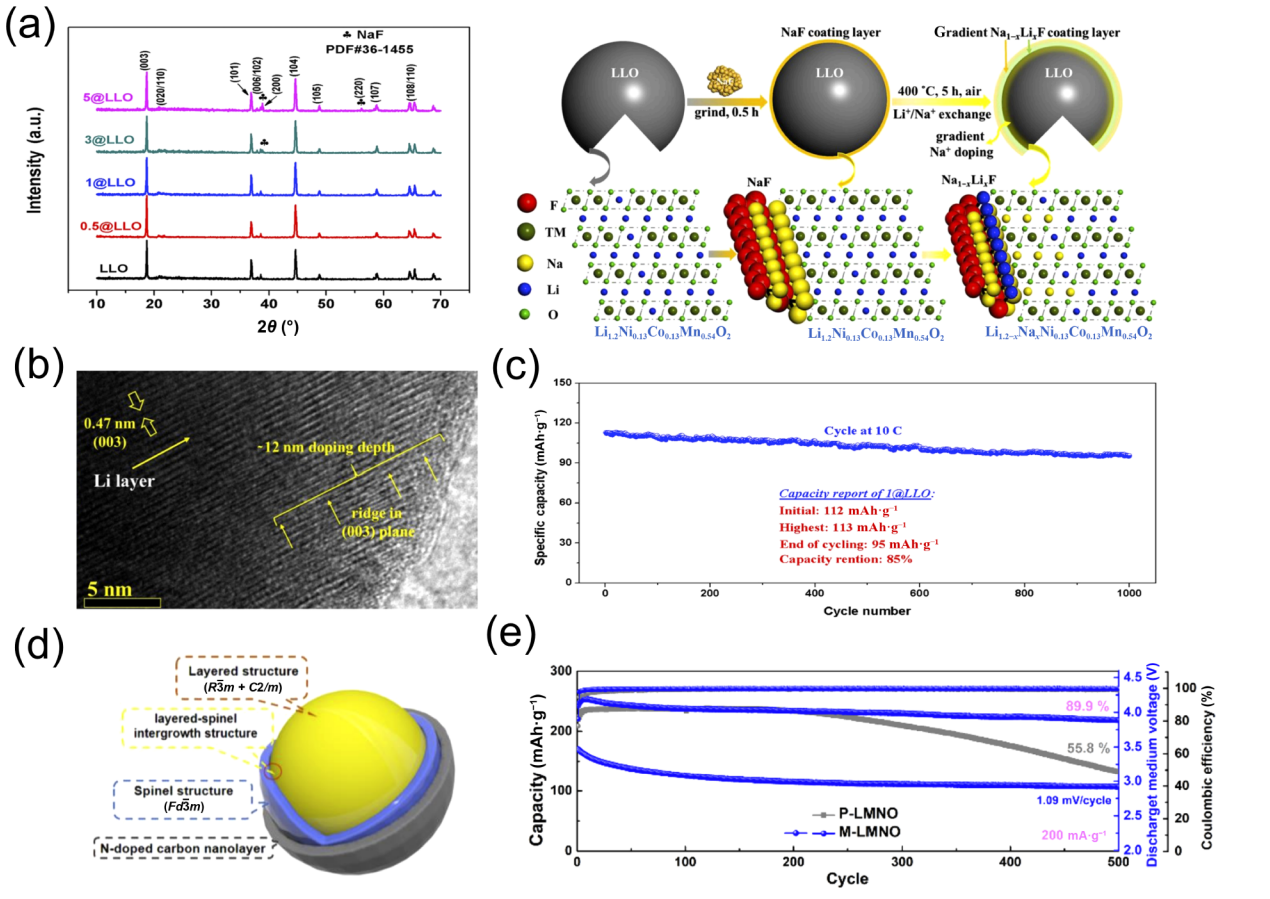

Figure 9 (a) XRD patterns of pristine and NaF modified LLOs with different amount and schematic diagram of Li^+/Na^+ exchange process. (b) HRTEM image and (c) cycling performance at 10 C for NaF modified LLOs. Reproduced with permission from Ref. [82], © Elsevier Ltd. 2019. (d) Schematic illustration of N-doped carbon coated at the surface of LRMNO. (e) Ultra-long cycling performance and corresponding discharge median voltage and Coulombic efficiency at 1 C for pristine and N-doped carbon coating LRMNO. Reproduced with permission from Ref. [22], © Wiley-VCH Verlag GmbH & Co. KGaA, Weinheim 2020.

stability of HNLROs, the reduction in capacity is easily seen (192.5 $mAh·g^{-1}$ for $Li_{1.2}Ni_{0.4}Mn_{0.4}O_2$ versus 244 $mAh·g^{-1}$ for $Li_{1.2}Ni_{0.2}Mn_{0.6}O_2$ at 0.1 C) [72, 88]. The capacity decrease of HNLROs could be attributed to the deteriorated side reactions between Ni^{4+} and electrolytes as a consequence of the reduced reversible anionic redox associated with the decreased Li_2MnO_3-like component and/or the difficulty of electrochemical activation [16, 44, 89]. In addition, HNLROs normally show a relatively lower ICE and a far higher charge potential (~ 4.8 V) compared with conventional $LiMO_2$ oxides (~ 4.3 V) [33]. Thus, a high potential is required to activate the anionic oxygen redox of the Li_2MnO_3-like component in HNLROs for higher capacity, which would also cause a large irreversible capacity loss and thus a low ICE [23, 24, 55].

Therefore, escalating irreversible capacity and ICE of HNLROs is the primary target to pursue from the perspective of performance improvement. Generally, lattice doping [23, 24, 90], surface modification [16, 43, 80], new electrolyte additives exploration [18], and single crystal synthesis [32, 77, 91, 92] were proposed as effective ways to address the issues above.

3.2.1 *Single element modifications*

Mao D. et al. proposed a novel anti-evaporation loss engineering idea to increase the content of lattice lithium by doping trace Na^+ or K^+ into $Li_{1.2}Ni_{0.32}Mn_{0.48}O_2$ for significant performance improvement via a facile expanded graphite template-sacrificed approach (Figs. 10(a)–10(d)) [24]. Both the Na- and K-doped samples exhibited excellent rate capability such as 217, 201, 162, and 141 $mAh·g^{-1}$ as well as 212, 191, 162, and 133 $mAh·g^{-1}$ for 0.5, 1, 5, and 10 C, respectively, and high capacity retentions such as 93% and 89% after 200 cycles at 1 C, respectively, in sharp contrast with 74% for the pristine sample, which are quite outstanding for HNLOs (Fig. 10(e)) [24]. The greatly improved performance could be attributed to the increased effective Li content and *C2/m* component in the lattice via Li anti-evaporation-loss engineering, the expanded Li slabs, and the pillaring effect (Fig. 10(f)) [24]. The differences in performance are believed to be associated with their different doping behaviors and threshold doping amounts caused by different radii between Na^+ and K^+ [24]. Guo L. et al. employed a facile sol-gel route to synthesize Mo-doped HNLROs for simultaneous achievement of both high reversible capacity and minor voltage decay (Fig. 10(g)) [55]. The superior performance could be ascribed to the reduced size of primary particles, the enhanced stability of lattice oxygen, and more Mn^{4+}/Mn^{3+} redox couples effectively activated via Mo doping during the electrochemical reactions (Fig. 10(h)) [55]. The trace dopings into the Li and Mn lattice sites endowed the modified HNLROs with steady discharge potential and high reversible capacity via different mechanisms and manners such as tailoring of morphologies, structures, and chemistries, which makes HNLROs very competent as next generation cathodes of LIBs (Fig. 10(i)). Similarly, a trace replacement of Mn by W for $Li_{1.2}Ni_{0.4}Mn_{0.4}O_2$ also led to significant performance improvement via elevating both the Li_2MnO_3-like superlattice component and Ni^{2+} proportion as a result of high valence W^{6+} (Fig. 11(a)) [23]. The increase in both capacity and ICE for a potential window of 2.0–4.8 V resulted from the reversible redox of more oxygen anions and reduced sizes of primary particles caused by trace W doping, as shown in Fig. 11(b) [23].

3.2.2 *Multiple element dopings*

Multiple element dopings into the same or different lattice sites are

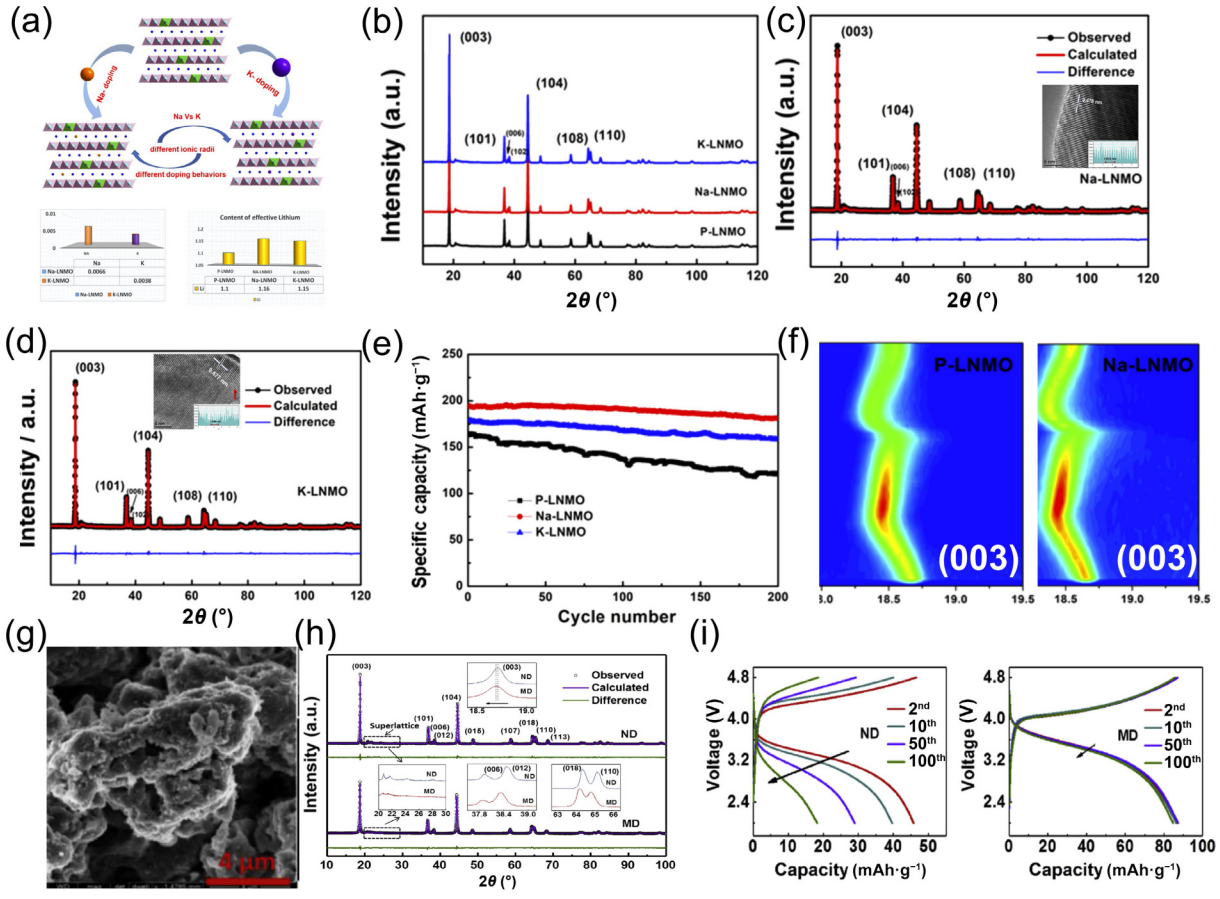

Figure 10 (a) Structural schematics of pristine and Na^+/K^+ doped HNLROs, (b) their XRD patterns, ((c) and (d)) Rietveld refinements, and (e) cycling performance at 1 C. (f) *In-situ* XRD color-coded contour maps of (003) peaks for HNLROs and Na-doped HNLROs. Reproduced with permission from Ref. [24], © American Chemical Society 2022. (g) SEM image of Mo-doped HNLROs. (h) XRD patterns and enlarged XRD patterns of pristine and Mo-doped HNLROs, and (i) their charge–discharge curves for different cycles within 2.0–4.8 V at 10 C. Reproduced with permission from Ref. [55], © Elsevier B.V. 2019.

also a commonly employed strategy of modifying the properties of various types of cathodes and anodes materials and further improving the performance. Trace co-doping of Fe cations and F anions into the transition metal and oxygen lattice sites of HNLROs, respectively, was proposed for remarkable performance improvement via an effective, simple, and up-scalable expanded graphites template-sacrificed approach (Fig. 11(c)) [90]. The co-doping effectively increased the Li–O bonds and the components of lower valence TMs for more effective activation of redox reactions relative to the doping of individual Fe cations or F anions, which therefore improved both rate capability and cycling stability in a synergistic manner (Fig. 11(f)) [90]. The Fe/F co-doped HNLROs exhibited an excellent cycling stability with a superior capacity retention of 90% after 200 cycles at 1 C, much higher than 64% for the pristine samples [90].

3.2.3 *Surface modifications*

As next generation promising candidate cathodes, surface modifications on HNLROs have been rarely reported in the past years, which are expected to be capable of enhancing the high-voltage performance including the escalation of both capacity and cycling stability at high voltages. HNLROs with a proper coating shell, such as coating HNLROs with LMROs shells, were controllably prepared to effectively improve their high-voltage cyclability (Fig. 11(e)) [93]. Taking $Ni(OH)_2$@$Mn(OH)_2$ as precursors and followed by a simple precipitation approach at 750 °C for 12 h, Jing Z. et al. successfully prepared a cathode material of layered HNLROs ($R\bar{3}m$) cores coated with thin monoclinic LMROs shells ($C2/m$) (CS-750) [93]. CS-750 thus prepared showed an outstanding high-voltage cycling stability (Fig. 11(f)) with a capacity retention as high as 96% after 100 cycles at 0.1 C [93]. *In-situ* high-resolution synchrotron-based XRD (HT-SXRD) technique revealed a continuous change in both position and intensity of reflections (003, 104, 018) and the absence of the splitting of reflections during the lithiation–delithiation processes for highly stable core–shell structures, as shown in Figs. 11(g) and 11(h). This unambiguously indicates quasi-solid-solution reactions during the electrochemical processes [93]. Moreover, all the reflections for CS-750 shifted to higher angles within the voltage range from 4.2 to 4.6 V during charging, implying a continuous shrinkage of unit-cells with the changes of −1.8% for c lattice constant and −5.9% for cell volume [93].

Since HNLROs have been derived primarily from LMROs by elevating the content of nickel, some of their natures, properties, and performances are quite similar. Therefore, many modification strategies capable of improving the performance of LMROs can be lent for HNLROs as well. With these approaches, the progress in performance improvement for HNLROs has been greatly made, including the suppression of voltage decay and the escalation of both capacity and high-voltage stability. For HNLROs, one of the primary targets may be focused on the escalation of capacity and high-voltage stability by increasing the cutoff voltage properly, as done for LCOs. Once the capacity of HNLROs is comparable with that of LMROs, the strengths would be more clearly seen. In this sense, HNLROs still have a long way to go, including the design of their chemical constituents and the exploration of novel modification strategies.

4 Cobalt-free layered LNOs cathodes

As discussed above, the Co-free cathode oxides with high

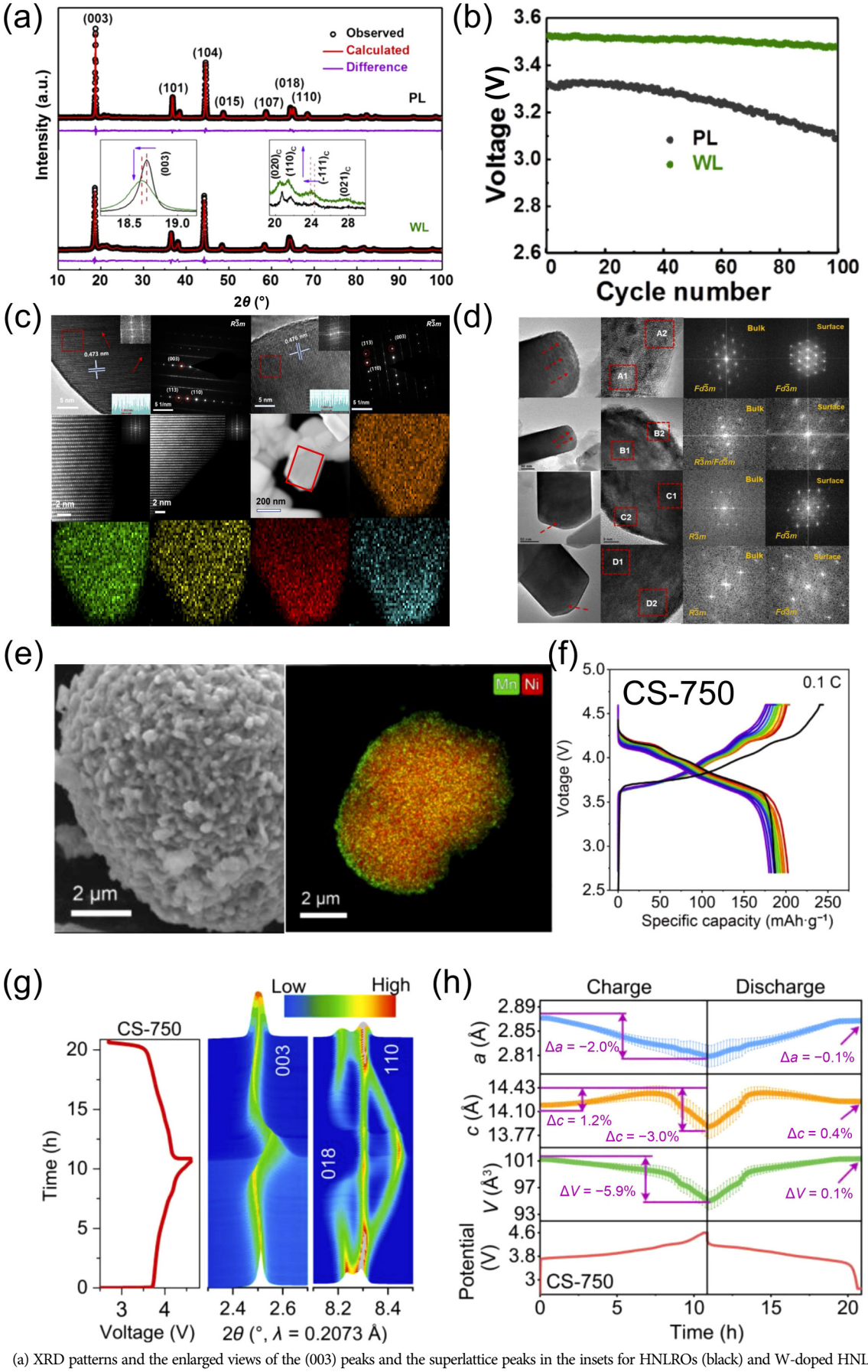

Figure 11 (a) XRD patterns and the enlarged views of the (003) peaks and the superlattice peaks in the insets for HNLROs (black) and W-doped HNLROs (green), and (b) their cycling performance at 10 C. Reproduced with permission from Ref. [23], © Elsevier Ltd. 2021. (c) HRTEM, SAED images, and element mappings of Fe/F co-doped HNLROs. (d) TEM, HRTEM, and FFT images of pristine HNLROs, Fe-doped HNLROs, F-doped HNLROs, and Fe/F co-doped HNLROs after 200 cycles at 1 C. Reproduced with permission from Ref. [90], © American Chemical Society 2023. (e) SEM image, element mapping, and (f) high-voltage cycling performance between 2.7 and 4.6 V, and ((g) and (h)) crystallographic changes during the initial cycle within a voltage range of 2.7–4.6 V at 0.1 C for CS-750 s. Reproduced with permission from Ref. [93], © Elsevier B.V. 2023.

performance are undoubtedly the target to reach. Ni-based layered oxides with a high Ni content (Ni ≥ 80%) by replacing most Co based on LCOs are currently one of mainstreams for both fundamental research and practical applications because of their lower cost, higher specific capacities, and energy densities [15, 42, 94–96]. However, many issues would also arise for LNOs such as morphological damage [47, 97], structural transformation from layered to spinel-like, and/or rock salt-type phases, especially at the surface [15, 48, 56, 98, 99], parasitic reactions with electrolyte and thermal instabilities associated with high reactivity of Ni ions [56, 100]. Similar to other Co-based/Co-reduced layered oxides, elemental doping/substitutions (W [26, 100, 101], Fe [49], Ti [34], and Al [102]), surface modifications (ZrO [103], Al_2O_3 [104], and SiO_2 [105]), and morphology design are the most effective and common ways capable of easing these issues.

4.1 Heteroatoms doping

Trace or minute element doping is one of the most common ways of improving the performance of LNOs. Trace Al or/and Co could be introduced into LNOs to form $LiNi_{0.95}Co_{0.05}O_2$ (NC95), $LiNi_{0.95}Al_{0.05}O_2$ (NA95), and $LiNi_{0.95}Co_{0.03}Al_{0.02}O_2$ (NCA95) with similar particle morphologies for investigations of the roles played by Al and Co. (Fig. 12(a)) [106]. Individual trace Al or Co doping led to close capacity retentions for 500 cycles at 2C within a voltage window of 2.5–4.2 V in full cells at 45 °C, such as 54.1% for NA95 and 56.5% for NC95 [106]. The increase of Al amount would improve the capacity retention up to 75% (Fig. 12(b)) as a result of more effective suppression of charge transfer resistance increase, side reactions, and surface degradation [106]. Also, less severe cracking of particles was observed for NA92, suggesting the effective prevention of both surface and bulk degradation by the increased Al [106]. Therefore, $LiNi_xAl_{1-x}O_2$ doped with Al may be one of promising Co-free Ni-rich layered oxide electrodes because of their outstanding performance [106]. Although Co substitution is effective in suppression of bulk degradation and Al substitution is effective in suppressing surface degradation, their total quantity and ratio upon co-doping also need to be taken into considerations carefully and optimized, which is very important for performance improvement [107]. W was also doped into $LiNiO_2$ successfully to modify both crystal structure and primary particle morphology via an ammonium tungstate flux [100]. W dopants were revealed to occupy the Ni site and could concurrently induce the migration of Ni^{2+} to the Li site (Fig. 12(c)) [100]. At lower temperatures of synthesis, tungsten was found capable of inhibiting the growth of primary particles [100]. The substitution of W^{6+} for Ni^{3+} at the 3a site would trigger the presence of Ni^{2+} at the Li site for the sake of requirement of charge neutrality (Fig. 12(d)) [100]. Manthiram A. et al. pioneeringly performed the challenging work on rational compositional design of high-Ni layered oxides within a limited range of doping concentrations (< 10%) by exploring the intrinsic roles of critical dopants such as Co, Mn, and Al in LNOs [97].

4.2 Surface modification

Surface modifications/treatments with the introduction of proper active materials can be normally used for the suppression of oxygen loss by different degrees during electrochemical processes. However, upon introducing a coating layer with a proper thickness at the surface of LNOs particles, whether the layer is coherent or incoherent with LNOs would be dependent on the similarity of their crystalline structures and the match degree of their lattice parameters [25]. Normally, with a coherent interface between the coated layer and LNOs, the ionically conductive layer with great inertness to electrolyte is much more preferred, which would be favorable for ionic transport and surface stabilization and thus improve the performance more significantly [25, 51].

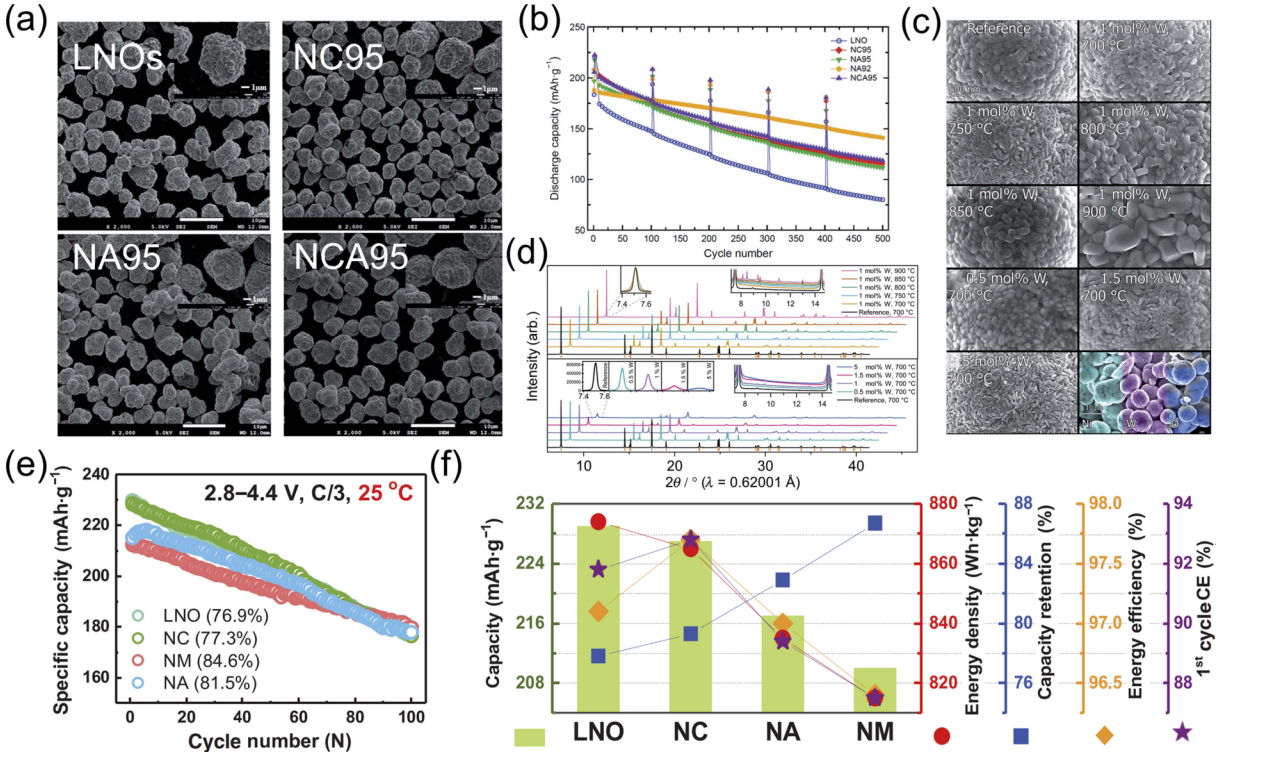

Figure 12 (a) SEM images of LNOs, NC95, NA95, and NCA95 and (b) their cycling performance within a potential range of 2.5–4.2 V at 2 C and at 45 °C. Reproduced with permission from Ref. [106], © The Royal Society of Chemistry 2021. (c) SEM images of W-doped LNOs with different W amount and EDX spectra for the 1 mol% W-doped sample. (d) XRD profiles of W-doped LNOs prepared with varied synthesis temperature (top) and W contents (bottom). Reproduced with permission from Ref. [100], © The Royal Society of Chemistry 2022. (e) Cycling performances of LNOs, NC, NM, and NA within a potential range of 2.8–4.4 V at 0.3 C, and (f) comparisons of their capacity, energy density, capacity retention, energy efficiency, and ICE. Reproduced with permission from Ref. [97], © Wiley-VCH GmbH 2023.

Chen et al. explored the formation of a disordered layered $Li_{1-x}Ni_{1+x}O_2$ ($R\bar{3}m$) at the surface of LNOs primary particles with the controlled Li contents during high-temperature solid-state reactions (Fig. 13(a)) [25]. An ordered surface (LNO-OS) for a macroporous architecture within the agglomerates of LNO primary particles was demonstrated using synchrotron-X-ray 3D imaging and spectroscopic techniques after only 40 cycles, accompanied by the reduction of nickel ions at the surface of primary particles across the entire secondary particle (Fig. 13(b)) [25]. Such chemimechanical degradation accelerates the deterioration of LNO-OS cathodes [25]. In contrast, the disordered surface, which serves as a self-protective layer to alleviate the oxygen loss, possesses the same layered rhombohedral structure ($R\bar{3}m$) as the inner core of primary particles of the $Li_{1-x}Ni_{1+x}O_2$ ($x \approx 0$) [25]. Only slight changes in the nickel valence state and interior architecture of LNO with a thin disordered surface layer (LNO-DS) after cycling were observed, which mainly arose from an improved robustness of the oxygen framework at the surface [25]. By introducing small amount of niobium, the surface and structure degradation of LNOs could be effectively suppressed via a facile solution-mediated Nb incorporation method [48]. Full cells of niobium-treated LNO paired with a graphite anode retained 81.8% of their initial capacities after 500 cycles for 0.5 C charge and 1 C discharge compared with 73.2% for untreated LNO (Fig. 13(c)) [48]. The introduction of Nb was demonstrated to form Nb-contained oxide layers which can enhance lithium-ion diffusion kinetics and reduce the loss of active materials against long-term cycling (Figs. 13(d) and 13(e)) [48]. The enhanced structural integrity and thus electrochemical performance of the niobium-treated $LiNiO_2$ are correlated to decreased nanopore defects formed during cycling compared with the untreated $LiNiO_2$ [48].

4.3 Morphology design

Surface modifications strategies are normally difficult to achieve the desired morphologies of primary and secondary particles not only for LNOs but also for other electrode materials. By designing a desired architecture such as porous aggregates composed of primary nanoparticles, a proper preparation approach needs to be carefully selected for realization of the morphology, say, a conventional co-precipitation method [5, 15]. Undoubtedly, the performance of an electrode material would be determined by not only the intrinsic natures of primary particles but also the properties of secondary particles assembled by primary particles, such as particle sizes and their distribution, porosity, and grain boundaries which are difficult to be separated from one another for investigations of individual roles [4, 5, 32, 42]. Kim M. et al. prepared uniform and well-faceted SC-LNO particles with different shapes for exploring the dependences of rate performance and cycling stability on particle morphology and surface [99]. Octahedron-shaped SC-LNO with the (012) facets was revealed to show the better rate capability and improved stability during kinetically slow anodic processes in the region up to 3.5 V, and cubic-shaped SC-LNO with the (104) facets had the superior cycling stability, especially upon cycling at a high upper cutoff voltage of 4.6 V (Fig. 14) [99]. Improvement in cycling stability is correlated with reduced surface reconstruction and preferential LiF formation through the interaction with the electrolyte at the (104) surface [99]. These studies not only demonstrate the important roles of morphology and surface design for primary particles but also provide in-depth understanding about achievement of desirable properties and electrochemical performance of LNO-based derivatives cathodes [99].

With the increased interest in high nickel layered oxides cathodes in recent years, the world-wide research on layered $LiNiO_2$-based derivatives has been rekindled again because of potentially high capacity and relatively low cost, especially compared with LCOs. However, their complicated phase transitions and structure/surface instability during electrochemical processes are sufficiently recognized as well. Fortunately, both capacity and cycling stability have been remarkably elevated via surface modifications, trace element doping, and proper morphological design. However, at present, their practical applications may be restricted predominantly by the most critical issue, safety. In this sense, upon developing novel strategies, not only performance improvement but also high enough safety need to be required.

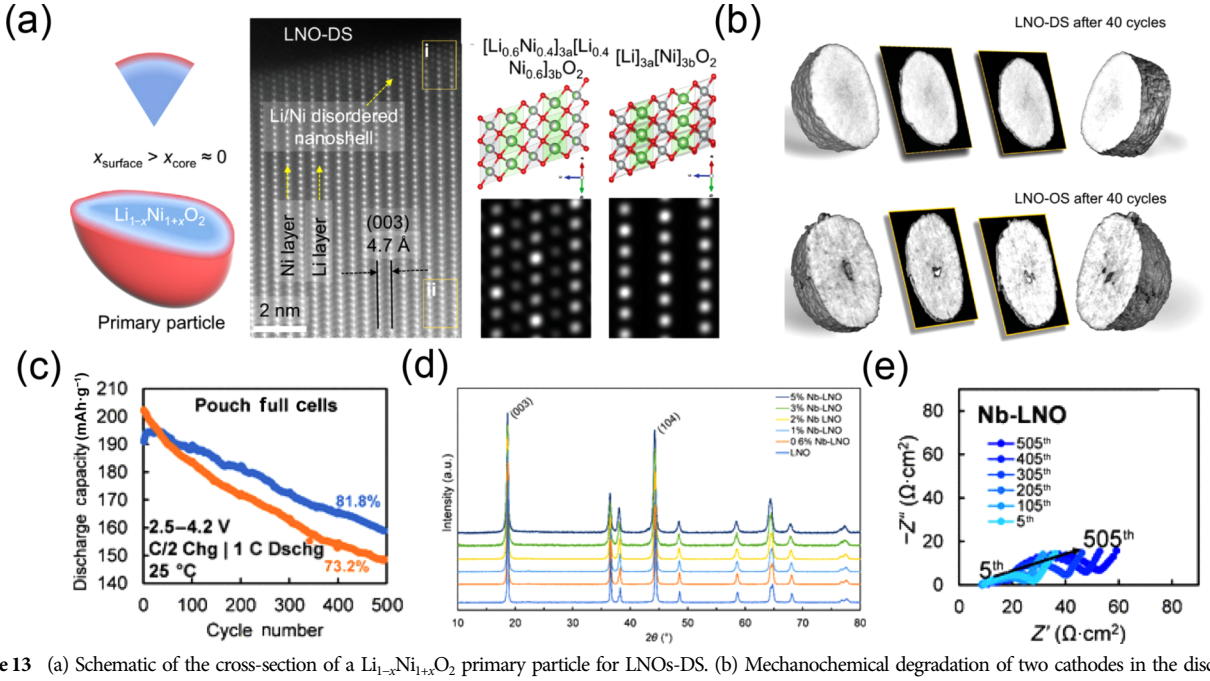

Figure 13 (a) Schematic of the cross-section of a $Li_{1-x}Ni_{1+x}O_2$ primary particle for LNOs-DS. (b) Mechanochemical degradation of two cathodes in the discharged state after over 40 cycles at 0.1 C for LNOs-DS (top) and LNOs-OS (bottom). Reproduced with permission from Ref. [25], © Chen, J. N. et al. 2022. (c) Cycling performance of pristine LNOs and Nb-LNOs. (d) X-ray diffraction patterns of LNOs and Nb-LNOs. (e) Impedance spectra of Nb-LNOs in pouch full cells. Reproduced with permission from Ref. [48], © American Chemical Society 2023.

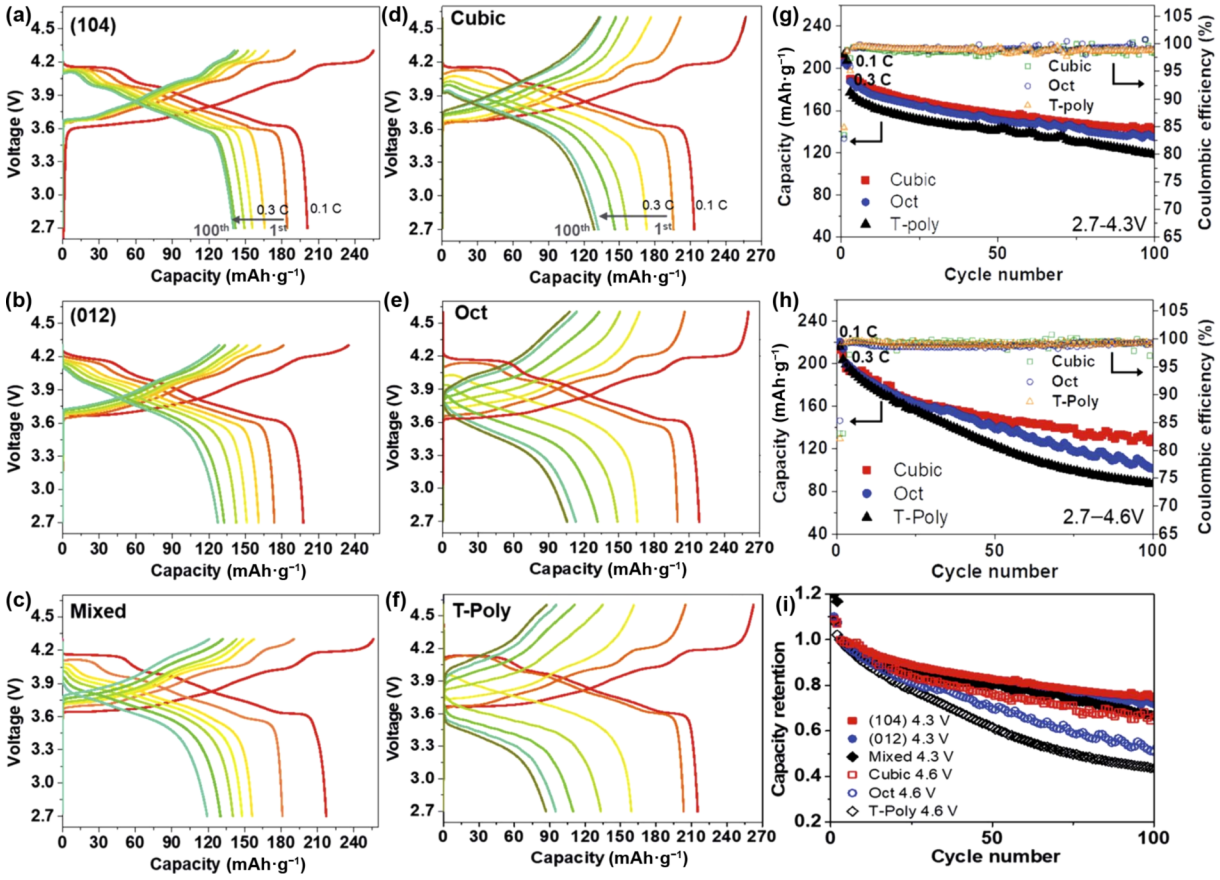

Figure 14 ((a)–(f)) Voltage profiles of different LNOs within a potential range of 2.7–4.3 V ((a)–(c)) and 2.7–4.6 V ((d)–(f)) for 100 cycles with first two cycles at 0.1 C and rest cycles at 0.3 C. (g) Discharge capacity and Coulombic efficiency as a function of cycle number within a potential window of 2.7–4.3 V and (h) 2.7–4.6 V, and (i) capacity retention as a function of cycle number (i). Reproduced with permission from Ref. [99], © The Royal Society of Chemistry 2022. Figure 14 adapted with permission from Ref. [99], © 2022 The Royal Society of Chemistry.

5 Potential anodes for layered oxides

For high-performance LIBs with high capacity, energy density, and superior cycling stability, not only cathode materials with desired performance but also proper anodes to pair with are indispensable [96]. With the progress of novel cathodes with high performance, potential anodes with great safety, stability, and high capacity to pair with are also explored [107–110]. In reality, it is greatly challenging to hunt for proper anodes which can well match with different cathodes [111–113]. Some of the representative anodes are shown in Fig. 15.

5.1 Carbon-based anodes

Of all the types of anode materials discovered so far, the carbon-based anodes seem to be the most promising and are already commercialized [114, 115]. However, traditional graphitic carbon anodes have a relatively low theoretical capacity of 372 mAh·g^{-1} with a low lithiation potential which corresponds to a saturated lithium composition of LiC_6 regardless of a low Li-ion transport rate (10^{-12}–10^{-14} cm^2·s^{-1}) due to the regular arrangement of graphite layers [116, 117]. Carbon anodes with this capacity appear to be quite good for layered $LiCoO_2$ cathodes, but not qualified for those novel cathodes of Li-rich layered oxides with theoretical capacities higher than 400 mAh·g^{-1}. To address the issue of insufficiently high capacities of anode, great endeavor was made to explore novel anodes with both high capacity and power such as hard carbons (HCs) which are potential for future LIBs technologies [118–120]. HCs have a structure of "house of cards" with randomly packed graphite layers which allow Li ions to reside into their nanovoids or to be absorbed at the surfaces of the graphite sheets, and thus contribute to an excess Li storage capacity [110, 114]. Aside from this larger utilizable capacity, HCs have a larger interplanar distance (0.36–0.38 nm) than that of graphite (≈ 0.33 nm), which can further facilitate fast transport of Li ions in the graphitic lattices, thereby enabling high-rate capability particularly desirable for power Li-ion batteries [120]. Despite these attractive advantages, HCs still have a serious drawback of ICE as low as 50%–60% [121, 122], arising from a large initial capacity loss, due to the large surface area of its disordered graphitic texture [117]. This large initial capacity loss consumes the Li ions in the electrolyte and needs to be compensated by loading an excess amount of cathode materials, and thus considerably weakens its capacity strength again [116, 123]. Consequently, this low ICE can significantly affect negatively the cycling stability which would give rise to serious challenges for practical applications of LIBs [124].

Therefore, it is imperative to develop new carbon-based materials to meet the requirements of both the ICE and rate capability. In fact, various prelithiation strategies have been proposed to escalate the ICE of HCs and thus improve the performance of LIBs upon employing LCOs as a cathode [19, 120]. However, few studies are reported to increase ICE without prelithiation from a viewpoint of structure engineering. This would be expected to be one of important promising aspects which will be discussed on the basis of high ICE prelithiation-free HC-based carbon anodes prepared with some potential synthesis methods. Upon pairing with some cathodes, the full cells show excellent performance.

Similar to cathodes materials, morphology control, surface modifications, and heteroatoms doping are still three types of effective approaches for performance improvement of novel carbon-based anodes normally with a tradeoff between ICE and

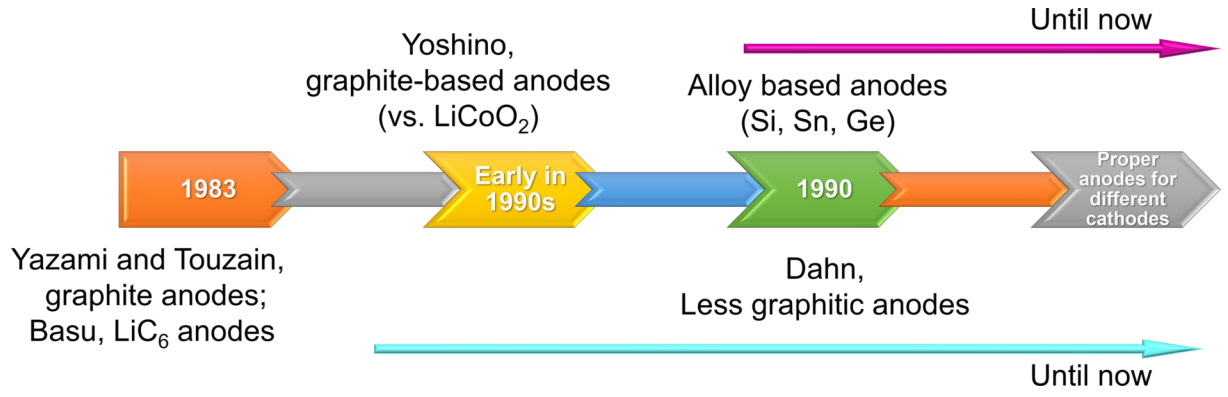

Figure 15 The milestones of anodic materials for LIBs.

rate-capacity [125]. Chen K. et al. fabricated hybrid anodes with uniform mixtures of graphite and hard carbon, using industrially-relevant multi-layer pouch cells (> 1 Ah) and electrode loadings (3 mAh·cm^{-2}) [126]. By controlling the graphite/hard carbon ratios, the performance of batteries can be systematically tailored to achieve both high-energy density and highly efficient fast charging [126]. Pouch cells with the optimized hybrid anodes retained 87% and 82% of their initial specific energies after 500 cycles at high rates of 4 and 6 C, respectively (Figs. 16(a) and 16(b)) [126]. This is significantly higher than 61% and 48%, the specific energy retentions with graphite anodes only under the same conditions [126]. The enhanced performance is attributed to the improved homogeneity of the reaction current throughout the hybrid anode, which is supported by continuum-scale modeling [126]. This process is directly compatible with existing roll-to-roll battery manufacturing, representing a scalable pathway to fast charging [126]. Xu H. et al. developed hierarchical carbon-based hollow frameworks embedded with cobalt nanoparticles for performance enhancement through pyrolyzing core–shell ZIF-8@ZIF-67 polyhedrals synthesized via a seed mediated growth method (Fig. 16(c)) [127]. The resultant hollow frameworks are composed of the N-doped carbon as the inner shells and the porous graphitic carbon embedded with cobalt nanoparticles as the outer shells (Fig. 16(d)) [127]. Benefiting from the unique hollow architecture with large surface area and good electrical conductivity, the anode materials exhibit good electrochemical performance with improved specific capacities, high-rate capability, and cycling stability [127]. More importantly, the quantitative kinetic analysis revealed the crucial contributions of N doping and the porous structure of graphitic carbon with cobalt nanoparticles for boosting the performance of carbon-based materials [127]. The rational design of the unique carbon-based architecture and the understanding of the underlying mechanism for the charge storage process are crucial to construction of advanced carbon-based materials for high-performance LIBs (Fig. 16(e)) [127]. The transition from layered graphite to 3D crumpled graphene (CG) was demonstrated to effectively trigger the surface-controlled charge storage, which thus dramatically improved the Li-ion charge storage kinetics and structural stability at low temperatures [128]. The structure-controlled CG anodes prepared via a one-step aerosol drying process showed a remarkable rate-capability by delivering about 206 mAh·g^{-1} at a high current density of 10 A·g^{-1} at room temperature (Fig. 16(f)) [128]. At an extremely low temperature of −40 °C, CG anode still exhibits a high capacity of about 154 mAh·g^{-1} at 0.01 A·g^{-1} with excellent rate-capability and cycling stability (Figs. 16(g) and 16(h)) [128]. Furthermore, both theory and experiments revealed that the superior performance of CG anode stems predominantly from the surface-controlled charge storage mechanism at various defect sites [128]. This study supported the effective utilization of the surface-controlled charge storage for improvement of both charge storage kinetics and stability at low temperatures in terms of a promising strategy of structure-controlled graphene.

As a typical and already commercialized anode material, great progress has been made in carbon which can be paired with multiple cathodes. Although ion-intercalation-type commercialized graphitic carbon with different morphologies could even deliver the capacities close to their theoretical value, for commercial applications, the capacities are still an obstacle to the escalation of energy-density for LIBs. Therefore, the emergence of HC may bring about the promise for high energy density LIBs as a candidate anode. However, several issues regarding solid-electrolyte interphase (SEI), ICE, and safety remain to be addressed. This may bring about great challenges for commercialization and practical applications of HC-based LIBs.

5.2 Silicon-based anodes

Silicon (Si)-based anodes have been the promising candidates as another type of most prospective alternative for commercial graphite because of their ultrahigh theoretical capacity of 4200 mAh·g^{-1} corresponding to fully lithiated $Li_{22}Si_5$ alloys [129–131]. However, their challenges for practical applications are mainly focused on large volume expansion as high as about 420% during Li^+ insertion/deinsertion and low intrinsic conductivity which leads to materials pulverization, electrodes failure, and unstable SEI [132, 133]. To address the typical issues of Si anodes, especially volume expansion, massive efforts have been made to avoid materials pulverization via designing silicon nanostructures [134–136], improve cycling stability through adopting novel structures of SiO/SiO_x-based anode materials [137–139], and increase electronic/ionic conductivities through utilizing advanced electrolyte additives and novel binders [140, 141].

Porous silicon can be divided into nano-sized structures and micron-sized structures [136, 142, 143]. Nano-sized silicon anodes with large specific surface areas can effectively relieve the volume expansion of silicon to avoid cracking of materials and thus enhance the cycling performance, which is one of mainstreams for silicon anodes [125, 129]. Si with micro-sized structures receives much less attention because of much poorer performance relative to that for Si with nanosized-structures, and will not therefore be discussed extensively here. Collins et al. achieved Si nanowires (NWs) with high loading (> 1.6 mg·cm^{-2}) by seeding the growth from a dense array of $Cu_{15}Si_4$ NWs using tin seeds (Fig. 17(a)) [142]. A one-pot synthesis approach involves the direct growth of CuSi NWs on Cu foil that acts as a textured surface for Sn adhesion and Si NW nucleation [142]. The high Si NWs loading can be realized by using high surface area CuSi NWs followed by secondary growth of Si NWs as branches from both Si and CuSi NW stems to form a dense Si active layer which was interconnected by an electrically conducting CuSi array (denoted

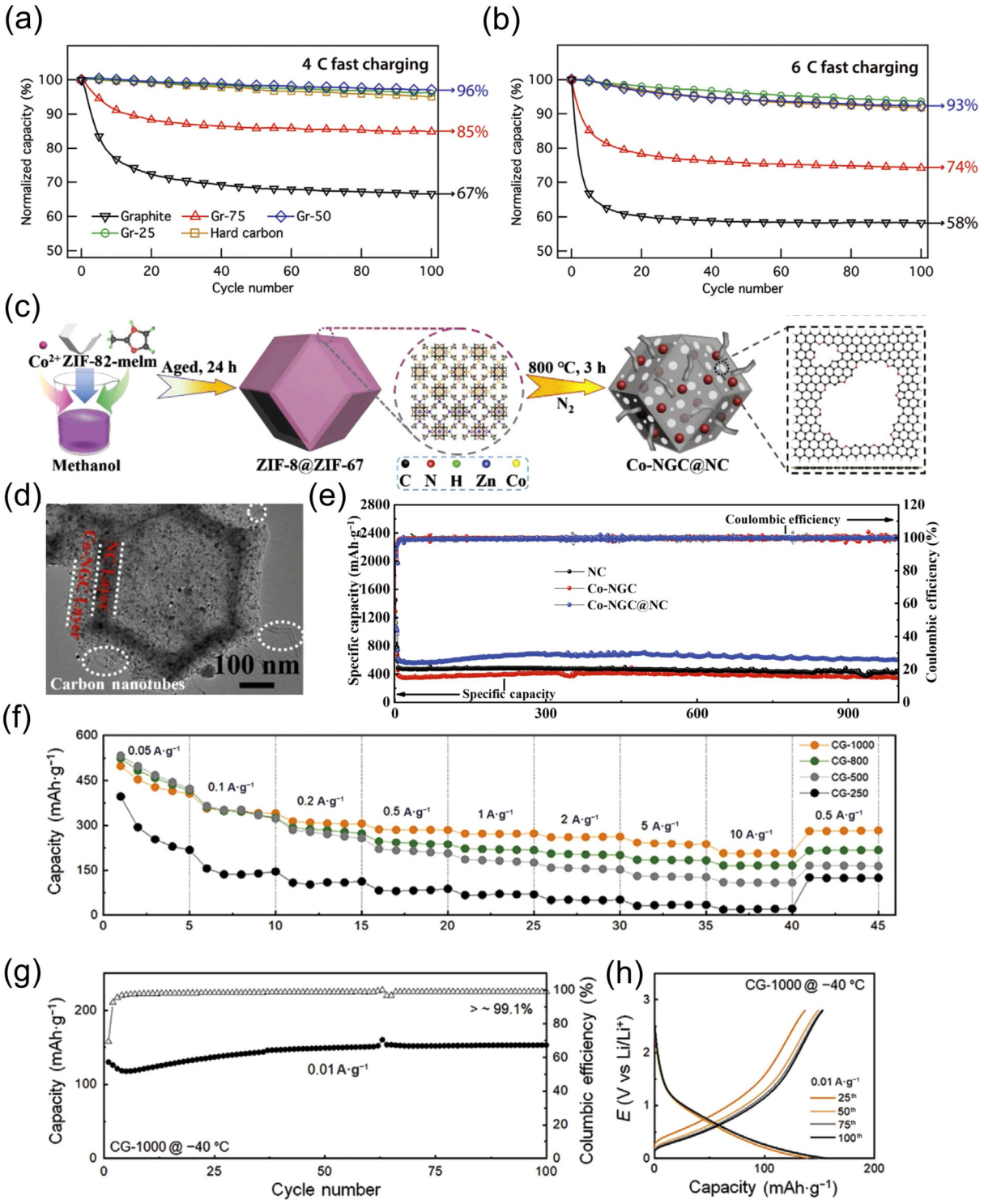

Figure 16 ((a) and (b)) Cycling stability (500 cycles) of different samples at high rates of 4 and 6 C, respectively. Reproduced with permission from Ref. [126], © Wiley-VCH GmbH 2020. (c) Schematic illustration of the preparation of Co-NGC@NC. (d) TEM image of Co-NGC@NC. (e) Cycling stability of NC, Co-NGC, and Co-NGC@NC at 1 C. Reproduced with permission from Ref. [127], © Wiley-VCH GmbH 2020. (f) Rate capacities of CGs achieved at different temperatures. ((g) and (h)) Cycling stability and corresponding GDC profiles of GC achieved at 1000 °C and tested at -40 °C. Reproduced with permission from Ref. [128], © Wiley-VCH GmbH 2021.

as Si/CuSi) [142]. When employed as Li-ion battery anodes, the Si/CuSi nest structure demonstrated impressive rate performance with 4.1 mAh·cm^{-2} at C/20, 3.1 mAh·cm^{-2} at C/5, and 0.8 mAh·cm^{-2} at 6 C (Fig. 17(b)) [142]. Also, Si/CuSi showed remarkable long-term stability with a steady areal capacity of 2.2 mAh·cm^{-2} after 300 cycles (Fig. 17(c)) [142]. Tian Y. et al. addressed the challenge by *in-situ* preparing magnesium-doped SiO_x ($SiMg_yO_x$) microparticles with stable structural evolution against Li uptake/release [136]. The homogeneous distribution of magnesium silicate in $SiMg_yO_x$ (Figs. 17(d) and 17(e)) contributed to building a bonding network inside the particle which raised the modulus of lithiated state and restrained the internal cracks due to electrochemical agglomeration of nano-Si [136]. The prepared micrometer-sized $SiMg_yO_x$ anode showed high reversible capacities, stable cycling performance, and low electrode expansion at high areal mass loading [136]. 21,700 cylindrical-type full cells based on $SiMg_yO_x$-graphite as anode and $LiNi_{0.8}Co_{0.15}Al_{0.05}O_2$ as cathode demonstrated a 1000-cycle

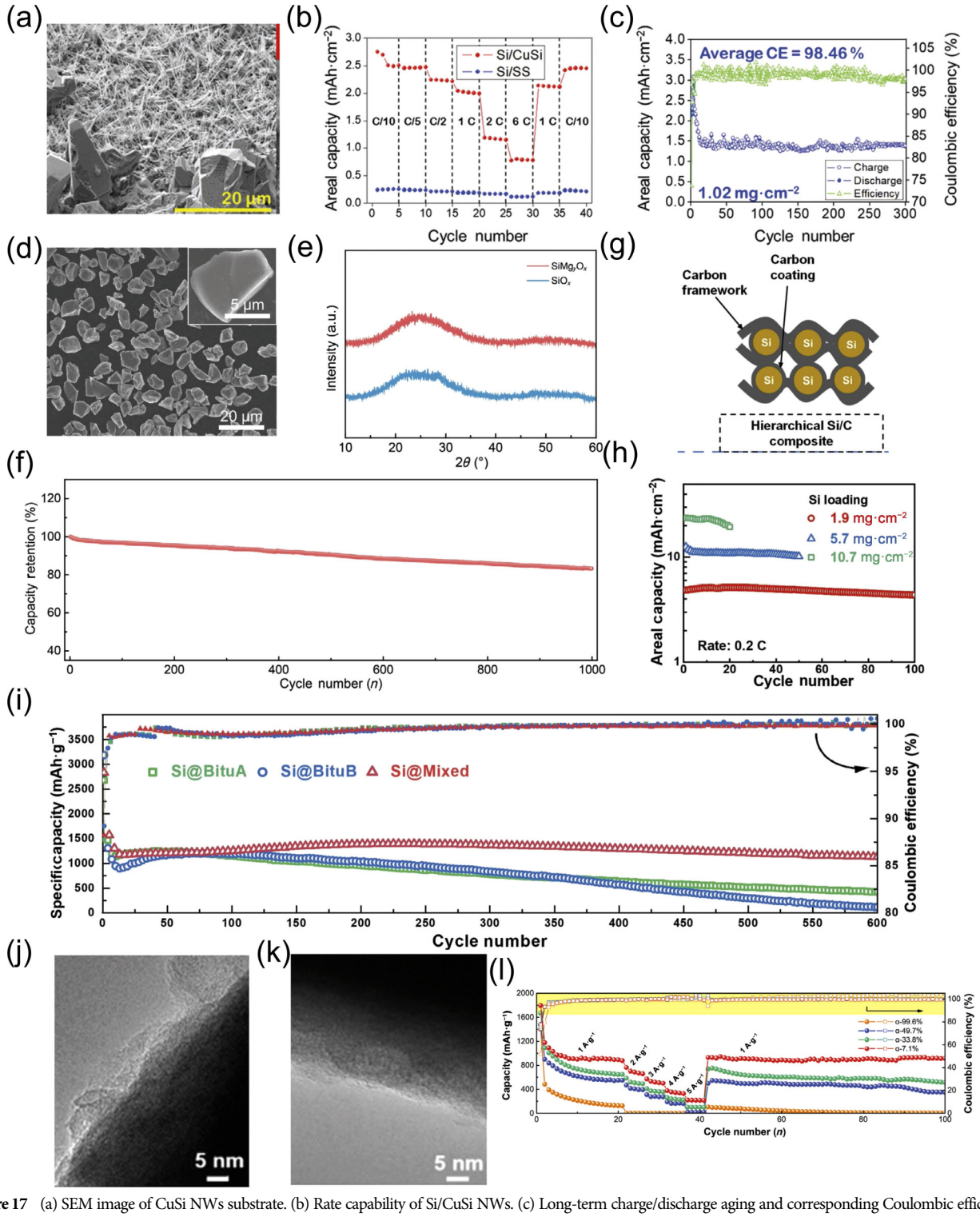

Figure 17 (a) SEM image of CuSi NWs substrate. (b) Rate capability of Si/CuSi NWs. (c) Long-term charge/discharge aging and corresponding Coulombic efficiency of Si/CuSi NWs with a Si loading mass of 1.02 mg·cm^{-2}. Reproduced with permission from Ref. [142], © Collins, G. A. et al. 2021. (d) SEM images of $SiMg_yO_x$@C, (the inset is a magnified image for single particle). (e) XRD patterns SiO_x and $SiMg_yO_x$. (f) Cycling performance of $SiMg_yO_x$@C-/$LiNi_{0.8}Co_{0.15}Al_{0.05}O_2$ pouch full cells. Reproduced with permission from Ref. [136], © Wiley-VCH 2022. (g) Structure illustration of Si/C nanocomposites. (h) Cycling performance for different Si loadings at 0.2 C. (i) Cycling performance of different Si/C samples at 1 C. Reproduced with permission from Ref. [133], © Wiley-VCH 2022. ((j) and (k)) TEM images of two SiO_x/C samples with different amount of carbon coatings. (l) Rate and cycling performance of different samples of SiO_x/C. Reproduced with permission from Ref. [135], © Wiley-VCH 2023.

operation life using industry-recognized electrochemical test procedures, which meets the practical storage requirements for consumer electronics and electric vehicles (Fig. 17(f)) [136]. This work provides insights into the reasonable structural design of micrometer-sized alloying anode materials toward realization of high-performance LIBs [136].

Furthermore, increasing the mechanical strength of anode materials and constructing rigid conductive networks can also minimize the effect of volume changes, which can improve the performance of Si-based anodes [132, 133, 144, 145]. The introduction of carbon-based materials with high mechanical strength and superior conductivity can enhance the conductivity of Si anode on one side, and alleviate the detrimental effect of silicon expansion as a protective layer on the other side [146, 147]. Hierarchical structures combining carbon coatings with other carbon-based conductive materials, such as carbon nanotubes

[131], carbon nanosheets [130, 148], and graphene [144], have been proposed to construct a robust protection layer to accommodate the volume change and a conductive network to maintain the integrity of electrode structures, which however usually sacrifices high capacity of Si [133, 149]. A hierarchical Si/C nanocomposite of robust carbon coatings and a firmly connected carbon framework on the silicon surface was synthesized by controlling the concentration of asphaltenes as carbon source and hence desired phase separation during the subsequent carbonization (Fig. 17(g)) [133]. The electrode made using this special Si/C nanocomposite exhibits a high reversible capacity of 1149 mAh·g^{-1} after 600 cycles (Fig. 17(i)) with a capacity retention of 98.5% and an area capacity as high as 23.8 mAh·cm^{-2} for a high mass loading over 10 mg·cm^{-2} (Fig. 17(h)), which is one of the highest area capacities reported with much more stable and prolonged operations [133]. Xiao Z. et al. explored in detail the mechanisms of surface modifications which enhanced the Si-based anodes performance in combination with carbon nanostructures [135]. The coating integrity may be a critical parameter influencing the performance of core–shell structure electrode materials (Figs. 17(j) and 17(k)) [135]. The coating integrity of SiO_x@C composite could be quantitatively described by an index of alkali solubility α proposed by using a selective alkali dissolution developed for tests. In detail, SiO_x dissolution loss had a significant impact on the overall electrode structure stability and interface properties, i.e., the coating integrity and thus the performance [135]. Because of the side reactions between uncoated active SiO_x and electrolyte, the quadratic decrease of initial Coulombic efficiency and increase of solid electrolyte interphase thickness with the rise of alkali solubility are closely related to the generated F content induced by active material loss. This was supported by the obvious linear rise of Li_2SiF_6 fraction which leads to the linear increase of interface impedance and volume expansion rate and thus accounts primarily for the performance deterioration (Fig. 17(l)) [135]. This work promotes the fundamental understanding about the interface failure mechanism and inspires rational high-performance electrode material design [135].

Lots of studies have been focused on the nanostructuring of Si for anodes materials because of its sufficiently high theoretical specific capacity. However, the combination with carbon via different manners to form various C/Si structures/architectures is indispensable for significant improvement of performance which not only can promote the electrical conduction but also alleviate the expansion of volume effectively. This would facilitate the adequate delivery of its capacity and the stabilization of long-term cycling via accommodating the volume changes to prevent from pulverization effectively. One should bear in mind that low ICE is one of the most critical points for C/Si nanostructures to be commercially applied. Novel strategies of prelithiation and prelithiation-free surface/structure engineering are still in urgent need. The C/Si nanostructures thus developed with desired performance could be well paired with LNOs/LCOs-derived layered oxides cathodes which would further increase the performance of LIBs and also promote the discovery of novel layered oxides cathodes simultaneously.

6 Conclusions and prospects

6.1 Layered LCO cathodic materials

Since the pioneering commercialization of LCO in 1991, especially for portable electronic devices, search for novel cathode materials with high energy density and low cost based on LCO has been continuing. Meanwhile, the research on the high-voltage performance of LCO, albeit with high Co content, is rekindled. The stabilization of structure at high voltages such as 4.5 V (vs. Li^+/Li) or above becomes the primary target in which more severe lattice oxygen loss, phase transition (CoO_2 → Co_3O_4), crack formation and particle pulverization, and interface side reactions at high voltages need to be addressed. Structural stabilization via various approaches including multi-element surface modifications and dopings was realized by different degrees to show much improved high-voltage performance, especially escalation of both capacity and cycling stability. Some of the approaches are cheap and up-scalable which can be employed for mass production. Moreover, novel approaches capable of improving the performance of LCOs are continuously to be hunted for. LCOs with superior high-voltage performance would still be the dominant cathodes for portable devices to promote the energy density of LIBs further. This would still be the focus of investigations about LCOs in near future.

6.2 Layered Co-reduced/Co-free cathodic materials

The scarcity and cost of cobalt really hinder large-scale applications of LCO, and numerous novel layered Co-reduced/Co-free cathodes with much lower cost have been discovered such as LNCMO series (NCM532, NCM622, NCM811, etc.), LNCAO, LMROs, HNLROs, and LNOs. Though the performance of these oxides has been improved by careful design of chemical, surface modifications, alien element dopings, and morphological and structural control, their insufficiently high safety and energy densities far from satisfactory still preclude their practical applications.

For LNCMO series, the capacity and energy density still need to be elevated though NCM532, NCM622, and NCM811 have been commercialized with a relatively small portion of market. However, the urgent point precluding their large-scale practical applications is still safety which originates from the instability of their structures leading to the abrupt heat release at relatively low temperatures. With the resolution of this issue, the NCMO series is expected to increase in the market rapidly and is the dominant target for commercialization at present. Also, the design of chemical constituents, surface and bulk modifications, and preparation approaches are still receiving much attention, which undoubtedly promotes in-depth understanding about electrochemical processes and thus triggers the emergence of novel strategies for performance improvement.

LMROs could deliver quite high capacities but show a severe voltage decay which is one of the most critical obstacles to their commercialization. In terms of chemical constituents tuning, surface and bulk modifications, and even structural and morphological tailoring via various effective approaches, the ICE and cycling stability have been enhanced remarkably which renders it possible to be applied in the future. However, HNLROs derived by replacing Mn by Ni with different quantities can effectively mitigate the voltage decay but deliver relatively low capacities and ICE. The potential of elevating capacity and cycling performance is giant because of large design flexibility of chemical constituents with a wide range along with various promising modification approaches. Moreover, as already done for LCOs, high-voltage strategies may hold for HNLROs to increase their capacities dramatically, which has been actually seen. Therefore, the leap in capacity achieved in the future may drive HNLROs faster for practical applications, which makes them very promising and competing for future generation cathode materials. Another new type of cathode materials may originate from structurally disordered Li-rich oxides based on LMROs by largely or fully substituting for Mn with alien multi-elements alongside with novel synthesis philosophies which may be revolutionized for cathode materials and thus LIBs in the future.

The interest in LNOs was rekindled owing to their higher capacities and far lower cost compared with LCOs. Their relatively low ICE and poor cycling stability as well as rate capability are seen to be improved obviously as well which are however far from satisfactory. The issue of safety characterized by large heat release at relatively low temperatures is probably paramount which cannot be circumvented as far as applications of LNOs. In reality, this issue may be closely related to the complicated multiple phase transitions during electrochemical processes. Accompanied by performance improvement via diversified strategies proposed, safety seems to receive less attention. Although LNOs were extensively explored via surface modifications, trace element dopings, morphological design, and adoption of efficient synthesis approaches, in-depth and thorough understanding about their complicated electrochemical processes still has a long way to go. Nevertheless, LNOs-based high nickel layered oxides are quite promising target cathodes for power LIBs in near future.

Although different cathodes above are encountered with different issues, some problems are quite common as well. First of all, their improved electrochemical performance is still far from satisfactory from the perspective of practical applications which needs to be further explored. Then, efficient and effective strategies for dramatic performance improvement, along with synthesis approaches, are normally difficult to be applied for mass production and commercialization. Also, their complicated electrochemical processes with underlying mechanisms for different modification and synthesis strategies are not fully understood, which may originate from the complexity of multiple phase transitions involved and the restriction of currently-available research paradigms and characterization methodologies. Finally, safety is of paramount issue for all the cathodes which needs to be well addressed via exploring novel approaches, especially for power LIBs.

6.3 Novel potential matched anodes

To match novel cathodes, novel potential anode materials are also quite in urgent need. The capacities of commercialized graphitic carbon are quite narrow for next-generation LIBs, which thus triggers the emergence of novel HC-based anodes with much higher capacities. Although capacities even higher than 1000 $mAh \cdot g^{-1}$ and superior cycling stability could be achieved, their common fatal shortcoming, i.e., quite low ICE (< 70% usually), is the biggest obstacle to their practical applications. Therefore, novel efficient and effective prelithiation strategies and surface engineering approaches are highly anticipated, which would be the primary target of research. Similarly, nanosized Si structures are faced with not only this issue but also large volume changes during electrochemical processes and far poorer conduction despite a very high theoretical capacity. The combination of carbon and nanostructured silicon including one-dimensional (1D) nanowires, two-dimensional (2D) nanosheets, and 3D hierarchically porous architectures, is definitely preferred for developing current and next-generation anode materials for high-energy-density LIBs. In addition, nanostructured C/Si-O composites are also promising anode materials for future high-performance LIBs. As a full system, proper match between cathodes and anodes with high safety and electrochemical performance is also quite important for the performance of LIBs. This requires not only analyzing the properties and natures of both cathodes and anodes and thus designing both LIBs structures and their fabrication processes but also carrying out a great many experiments to test their effectiveness.

Acknowledgements

This review is financially supported by the National Natural Science Foundation of China (No. 52172191) and Strategic Priority Research Program of the Chinese Academy of Sciences (No. XDB 36000000).

References

[1] Li, M.; Lu, J.; Chen, Z. W.; Amine, K. 30 years of lithium-ion batteries. *Adv. Mater.* **2018**, *30*, 1800561.

[2] Dong, Y. H.; Li, J. Oxide cathodes: Functions, instabilities, self healing, and degradation mitigations. *Chem. Rev.* **2023**, *123*, 811–833.

[3] Xiang, J. W.; Wei, Y.; Zhong, Y.; Yang, Y.; Cheng, H.; Yuan, L. X.; Xu, H. H.; Huang, Y. H. Building practical high-voltage cathode materials for lithium-ion batteries. *Adv. Mater.* **2022**, *34*, 2200912.

[4] Zeng, C.; Liang, J. N.; Cui, C.; Zhai, T. Y.; Li, H. Q. Dynamic investigation of battery materials via advanced visualization: From particle, electrode to cell level. *Adv. Mater.* **2022**, *34*, 2200777.

[5] Zheng, J. X.; Archer, L. A. Crystallographically textured electrodes for rechargeable batteries: Symmetry, fabrication, and characterization. *Chem. Rev.* **2022**, *122*, 14440–14470.

[6] Zhang, M. H.; Kitchaev, D. A.; Lebens-Higgins, Z.; Vinckeviciute, J.; Zuba, M.; Reeves, P. J.; Grey, C. P.; Whittingham, M. S.; Piper, L. F. J.; Van der Ven, A. et al. Pushing the limit of 3*d* transition metal-based layered oxides that use both cation and anion redox for energy storage. *Nat. Rev. Mater.* **2022**, *7*, 522–540.

[7] Rehnlund, D.; Wang, Z. H.; Nyholm, L. Lithium-diffusion induced capacity losses in lithium-based batteries. *Adv. Mater.* **2022**, *34*, 2108827.

[8] Nie, L.; Chen, S. J.; Liu, W. Challenges and strategies of lithium-rich layered oxides for Li-ion batteries. *Nano Res.* **2023**, *16*, 391–402.

[9] Muralidharan, N.; Self, E. C.; Dixit, M.; Du, Z. J.; Essehli, R.; Amin, R.; Nanda, J.; Belharouak, I. Next-generation cobalt-free cathodes—A prospective solution to the battery industry's cobalt problem. *Adv. Energy Mater.* **2022**, *12*, 2103050.

[10] Gou, X. X.; Hao, Z. K.; Hao, Z. M.; Yang, G. J.; Yang, Z.; Zhang, X. Y.; Yan, Z. H.; Zhao, Q.; Chen, J. *In situ* surface self-reconstruction strategies in Li-rich Mn-based layered cathodes for energy-dense Li-ion batteries. *Adv. Funct. Mater.* **2022**, *32*, 2112088.

[11] Zhang, W. J.; Chen, Y.; Xu, C. J.; Lin, C.; Tao, J. M.; Lin, Y. B.; Li, J. X.; Kolosov, O. V.; Huang, Z. G. Tunable electrical field-induced metal-insulator phase separation in $LiCoO_2$ synaptic transistor operating in *post-percolation* region. *Nano Energy* **2023**, *108*, 108199.

[12] Xu, S. Y.; Tan, X. H.; Ding, W. Y.; Ren, W. J.; Zhao, Q.; Huang, W. Y.; Liu, J. J.; Qi, R.; Zhang, Y. X.; Yang, J. C. et al. Promoting surface electric conductivity for high-rate $LiCoO_2$. *Angew. Chem., Int. Ed.* **2023**, *62*, e202218595.

[13] Tan, X. H.; Zhao, T. Q.; Song, L. T.; Mao, D. D.; Zhang, Y. X.; Fan, Z. W.; Wang, H. F.; Chu, W. G. Simultaneous near-surface trace doping and surface modifications by gas–solid reactions during one-pot synthesis enable stable high-voltage performance of $LiCoO_2$. *Adv. Energy Mater.* **2022**, *12*, 2200008.

[14] Tan, X. H.; Zhao, T. Q.; Guo, L. M.; Mao, D. D.; Song, L. T.; Liu, G. Y.; Wang, H. F.; Chu, W. G. Impact of electrolyte-permeable microcracks in secondary particles on performance of high nickel layered oxides: Negative or positive. *Mater. Today Energy* **2022**, *24*, 100942.

[15] Zhao, H.; Lam, W. Y. A.; Sheng, L.; Wang, L.; Bai, P.; Yang, Y.; Ren, D. S.; Xu, H.; He, X. M. Cobalt-free cathode materials: Families and their prospects. *Adv. Energy Mater.* **2022**, *12*, 2103894.

[16] Wang, J.; Yuan, Q.; Ren, Z. X.; Sun, C. H.; Zhang, J. F.; Wang, R.; Qian, M. M.; Shi, Q.; Shao, R. W.; Mu, D. B. et al. Thermochemical cyclization constructs bridged dual-coating of Ni-rich layered oxide cathodes for high-energy Li-ion batteries. *Nano Lett.* **2022**, *22*, 5221–5229.

[17] Jiang, M.; Danilov, D. L.; Eichel, R. A.; Notten, P. H. L. A review of degradation mechanisms and recent achievements for Ni-rich

cathode-based Li-ion batteries. *Adv. Energy Mater.* **2021**, *11*, 2103005.

[18] You, B. Z.; Wang, Z. X.; Shen, F.; Chang, Y. J.; Peng, W. J.; Li, X. H.; Guo, H. J.; Hu, Q. Y.; Deng, C. W.; Yang, S. et al. Research progress of single-crystal nickel-rich cathode materials for lithium ion batteries. *Small Methods* **2021**, *5*, 2100234.

[19] Jia, K.; Wang, J. X.; Ma, J.; Liang, Z.; Zhuang, Z. F.; Ji, G. J.; Gao, R. H.; Piao, Z.; Li, C.; Zhou, G. M. et al. Suppressed lattice oxygen release via Ni/Mn doping from spent $LiNi_{0.5}Mn_{0.3}Co_{0.2}O_2$ toward high-energy layered-oxide cathodes. *Nano Lett.* **2022**, *22*, 8372–8380.

[20] Zuo, Y. X.; Shang, H. F.; Hao, J. Z.; Song, J.; Ning, F. H.; Zhang, K.; He, L. H.; Xia, D. G. Regulating the potential of anion redox to reduce the voltage hysteresis of Li-rich cathode materials. *J. Am. Chem. Soc.* **2023**, *145*, 5174–5182.

[21] Zhang, K.; Qi, J. Z.; Song, J.; Zuo, Y. X.; Yang, Y. L.; Yang, T. H.; Chen, T.; Liu, X.; Chen, L. W.; Xia, D. G. Sulfuration of Li-rich Mn-based cathode materials for multianionic redox and stabilized coordination environment. *Adv. Mater.* **2022**, *34*, 2109564.

[22] Ding, X. K.; Luo, D.; Cui, J. X.; Xie, H. X.; Ren, Q. Q.; Lin, Z. An ultra-long-life lithium-rich $Li_{1.2}Mn_{0.6}Ni_{0.2}O_2$ cathode by three-in-one surface modification for lithium-ion batteries. *Angew. Chem., Int. Ed.* **2020**, *59*, 7778–7782.

[23] Guo, L. M.; Tan, X. H.; Mao, D. D.; Zhao, T. Q.; Song, L. T.; Liu, Y. L.; Kang, X. H.; Wang, H. F.; Sun, L. F.; Chu, W. G. Improved electrochemical activity of the Li_2MnO_3-like superstructure in high-nickel Li-rich layered oxide $Li_{1.2}Ni_{0.4}Mn_{0.4}O_2$ and its enhanced performances via tungsten doping. *Electrochim. Acta* **2021**, *370*, 137808.

[24] Mao, D. D.; Tan, X. H.; Guo, L. M.; Zhao, T. Q.; Fan, Z. W.; Song, L. T.; Zhang, Y. X.; Liu, G. Y.; Wang, H. F.; Chu, W. G. Lithium antievaporation-loss engineering via sodium/potassium doping enables superior electrochemical performance of high-nickel Li-rich layered oxide cathodes. *ACS Appl. Mater. Interfaces* **2022**, *14*, 19594–19603.

[25] Chen, J. N.; Yang, Y.; Tang, Y. S.; Wang, Y. F.; Li, H.; Xiao, X. H.; Wang, S. N.; Dewi Darma, M. S.; Etter, M.; Missyul, A. et al. Constructing a thin disordered self-protective layer on the $LiNiO_2$ primary particles against oxygen release. *Adv. Funct. Mater.* **2023**, *33*, 2211515.

[26] Zaker, N.; Geng, C. X.; Rathore, D.; Hamam, I.; Chen, N.; Xiao, P. H.; Yang, C. Y.; Dahn, J. R.; Botton, G. A. Probing the mysterious behavior of tungsten as a dopant inside pristine cobalt-free nickel-rich cathode materials. *Adv. Funct. Mater.* **2023**, *33*, 2211178.

[27] Tian, R. Y.; Liu, G. Y.; Liu, H. Q.; Zhang, L. N.; Gu, X. H.; Guo, Y. J.; Wang, H. F.; Sun, L. F.; Chu, W. G. Very high power and superior rate capability $LiFePO_4$ nanorods hydrothermally synthesized using tetraglycol as surfactant. *RSC Adv.* **2015**, *5*, 1859–1866.

[28] Tian, R. Y.; Liu, H. Q.; Jiang, Y.; Chen, J. K.; Tan, X. H.; Liu, G. Y.; Zhang, L. N.; Gu, X. H.; Guo, Y. J.; Wang, H. F. et al. Drastically enhanced high-rate performance of carbon-coated $LiFePO_4$ nanorods using a green chemical vapor deposition (CVD) method for lithium ion battery: A selective carbon coating process. *ACS Appl. Mater. Interfaces* **2015**, *7*, 11377–11386.

[29] Liu, H. Q.; Jiang, Y.; Tan, X. H.; Chen, J. K.; Guo, Y. J.; Wang, H. F.; Chu, W. G. Synthesis of well-crystallized, high-performance $LiNi_{0.5}Mn_{1.5}O_4$ octahedra as lithium-ion-battery electrode promoted by metal manganese powders. *Energy Technol.* **2017**, *5*, 414–421.

[30] Ji, H. W.; Urban, A.; Kitchaev, D. A.; Kwon, D. H.; Artrith, N.; Ophus, C.; Huang, W. X.; Cai, Z. J.; Shi, T.; Kim, J. C. et al. Hidden structural and chemical order controls lithium transport in cation-disordered oxides for rechargeable batteries. *Nat. Commun.* **2019**, *10*, 592.

[31] Lee, J.; Urban, A.; Li, X.; Su, D.; Hautier, G.; Ceder, G. Unlocking the potential of cation-disordered oxides for rechargeable lithium batteries. *Science* **2014**, *343*, 519–522.

[32] Zhang, W. J.; Yuan, C. H.; Zhu, J. F.; Jin, T.; Shen, C.; Xie, K. Y. Air instability of Ni-rich layered oxides-a roadblock to large scale application. *Adv. Energy Mater.* **2023**, *13*, 2202993.

[33] Ju, X. K.; Hou, X.; Liu, Z. Q.; Du, L. L.; Zhang, L.; Xie, T. T.; Paillard, E.; Wang, T. H.; Winter, M.; Li, J. Revealing the effect of high Ni content in Li-rich cathode materials: Mitigating voltage decay or increasing intrinsic reactivity. *Small* **2023**, *19*, 2207328.

[34] Kwon, S. N.; Song, M. Y.; Park, H. R. Electrochemical properties of $LiNiO_2$ substituted by Al or Ti for Ni via the combustion method. *Ceram. Int.* **2014**, *40*, 14141–14147.

[35] Zhang, J. X.; Wang, P. F.; Bai, P. X.; Wan, H. L.; Liu, S. F.; Hou, S.; Pu, X. J.; Xia, J. L.; Zhang, W. R.; Wang, Z. Y. et al. Interfacial design for a 4.6 V high-voltage single-crystalline $LiCoO_2$ cathode. *Adv. Mater.* **2022**, *34*, 2108353.

[36] Yang, X. R.; Wang, C. W.; Yan, P. F.; Jiao, T. P.; Hao, J. L.; Jiang, Y. Y.; Ren, F. C.; Zhang, W. G.; Zheng, J. M.; Cheng, Y. et al. Pushing lithium cobalt oxides to 4.7 V by lattice-matched interfacial engineering. *Adv. Energy Mater.* **2022**, *12*, 2200197.

[37] Qin, Y. P.; Xu, K. Y.; Wang, Q.; Ge, M. H.; Cheng, T.; Liu, M.; Cheng, H. Y.; Hu, Y. B.; Shen, C.; Wang, D. Y. et al. *In-situ* constructing a rigid and stable dual-layer CEI film improving high-voltage 4.6 V $LiCoO_2$ performances. *Nano Energy* **2022**, *96*, 107082

[38] Ruan, D. G.; Chen, M.; Wen, X. Y.; Li, S. Q.; Zhou, X. G.; Che, Y. X.; Chen, J. K.; Xiang, W. J.; Li, S. L.; Wang, H. et al. *In situ* constructing a stable interface film on high-voltage $LiCoO_2$ cathode via a novel electrolyte additive. *Nano Energy* **2021**, *90*, 106535

[39] Tan, X. H.; Mao, D. D.; Zhao, T. Q.; Zhang, Y. X.; Song, L. T.; Fan, Z. W.; Liu, G. Y.; Wang, H. F.; Chu, W. G. Long-term highly stable high-voltage $LiCoO_2$ synthesized via a solid sulfur-assisted one-pot approach. *Small* **2022**, *18*, 2202143.

[40] Liu, J. X.; Wang, J. Q.; Ni, Y. X.; Liu, J. D.; Zhang, Y. D.; Lu, Y.; Yan, Z. H.; Zhang, K.; Zhao, Q.; Cheng, F. Y. et al. Tuning interphase chemistry to stabilize high-voltage $LiCoO_2$ cathode material via spinel coating. *Angew. Chem., Int. Ed.* **2022**, *61*, e202207000.

[41] Huang, H.; Li, Z. Q.; Gu, S.; Bian, J. C.; Li, Y. Z.; Chen, J. J.; Liao, K. M.; Gan, Q. M.; Wang, Y. F.; Wu, S. S. et al. Dextran sulfate lithium as versatile binder to stabilize high-voltage $LiCoO_2$ to 4.6 V. *Adv. Energy Mater.* **2021**, *11*, 2101864.

[42] Zhang, Y. X.; Kim, J. C.; Song, H. W.; Lee, S. Recent achievements toward the development of Ni-based layered oxide cathodes for fast-charging Li-ion batteries. *Nanoscale* **2023**, *15*, 4195–4218.

[43] Jamil, S.; Li, C. M.; Fasehullah, M.; Liu, P.; Xiao, F. Y.; Wang, H.; Bao, S. J.; Xu, M. W. Ni/Li antisite induced disordered passivation layer for high-Ni layered oxide cathode material. *Energy Storage Mater.* **2022**, *45*, 720–729.

[44] Hyun, H.; Jeong, K.; Hong, H.; Seo, S.; Koo, B.; Lee, D.; Choi, S.; Jo, S.; Jung, K.; Cho, H. H. et al. Suppressing high-current-induced phase separation in Ni-rich layered oxides by electrochemically manipulating dynamic lithium distribution. *Adv. Mater.* **2021**, *33*, 2105337.

[45] Yan, P. F.; Zheng, J. M.; Liu, J.; Wang, B. Q.; Cheng, X. P.; Zhang, Y. F.; Sun, X. L.; Wang, C. M.; Zhang, J. G. Tailoring grain boundary structures and chemistry of Ni-rich layered cathodes for enhanced cycle stability of lithium-ion batteries. *Nat. Energy* **2018**, *3*, 600–605.

[46] Xu, G. L.; Liu, Q.; Lau, K. K. S.; Liu, Y. Z.; Liu, X.; Gao, H.; Zhou, X. W.; Zhuang, M. H.; Ren, Y.; Li, J. D. et al. Building ultraconformal protective layers on both secondary and primary particles of layered lithium transition metal oxide cathodes. *Nat. Energy* **2019**, *4*, 484–494.

[47] Deng, T.; Fan, X. L.; Cao, L. S.; Chen, J.; Hou, S.; Ji, X.; Chen, L.; Li, S.; Zhou, X. Q.; Hu, E. Y. et al. Designing *in-situ*-formed interphases enables highly reversible cobalt-free $LiNiO_2$ cathode for Li-ion and Li-metal batteries. *Joule* **2019**, *3*, 2550–2564.

[48] Ober, S.; Mesnier, A.; Manthiram, A. Surface stabilization of cobalt-free $LiNiO_2$ with niobium for lithium-ion batteries. *ACS Appl. Mater. Interfaces* **2023**, *15*, 1442–1451.

[49] Mohan, P.; Kalaignan, G. P. Structure and electrochemical performance of $LiFe_xNi_{1-x}O_2$ ($0.00 \le x \le 0.20$) cathode materials for rechargeable lithium-ion batteries. *J. Electroceram.* **2013**, *31*, 210–217.

[50] Yoon, C. S.; Jun, D. W.; Myung, S. T.; Sun, Y. K. Structural

stability of $LiNiO_2$ cycled above 4.2 V. *ACS Energy Lett.* **2017**, *2*, 1150–1155.

[51] Bianchini, M.; Roca-Ayats, M.; Hartmann, P.; Brezesinski, T.; Janek, J. There and back again-the journey of $LiNiO_2$ as a cathode active material. *Angew. Chem., Int. Ed.* **2019**, *58*, 10434–10458.

[52] Chen, J.; Zou, G. Q.; Deng, W. T.; Huang, Z. D.; Gao, X.; Liu, C.; Yin, S. Y.; Liu, H. Q.; Deng, X. L.; Tian, Y. et al. Pseudo-bonding and electric-field harmony for Li-rich Mn-based oxide cathode. *Adv. Funct. Mater.* **2020**, *30*, 2004302.

[53] He, W.; Liu, P. F.; Qu, B. H.; Zheng, Z. M.; Zheng, H. F.; Deng, P.; Li, P.; Li, S. Y.; Huang, H.; Wang, L. S. et al. Uniform Na^+ doping-induced defects in Li- and Mn-rich cathodes for high-performance lithium-ion batteries. *Adv. Sci.* **2019**, *6*, 1802114.

[54] Li, X.; Qiao, Y.; Guo, S. H.; Xu, Z. M.; Zhu, H.; Zhang, X. Y.; Yuan, Y.; He, P.; Ishida, M.; Zhou, H. S. Direct visualization of the reversible O^{2-}/O^- redox process in Li-rich cathode materials. *Adv. Mater.* **2018**, *30*, 1705197.

[55] Guo, L. M.; Tan, X. H.; Liu, S. N.; Wu, J. X.; Ren, J. C.; Zhao, T. Q.; Kang, X. H.; Wang, H. F.; Chu, W. G. Considerable capacity increase of high-nickel lithium-rich cathode materials by effectively reducing oxygen loss and activating $Mn^{4+/3+}$ redox couples via Mo doping. *J. Alloys Compd.* **2019**, *790*, 170–178.

[56] Zhang, H. L.; Liu, H.; Piper, L. F. J.; Whittingham, M. S.; Zhou, G. W. Oxygen loss in layered oxide cathodes for Li-ion batteries: Mechanisms, effects, and mitigation. *Chem. Rev.* **2022**, *122*, 5641–5681.

[57] Huang, Y. Y.; Zhu, Y. C.; Fu, H. Y.; Ou, M. Y.; Hu, C. C.; Yu, S. J.; Hu, Z. W.; Chen, C. T.; Jiang, G.; Gu, H. K. et al. Mg-pillared $LiCoO_2$: Towards stable cycling at 4.6 V. *Angew. Chem., Int. Ed.* **2021**, *60*, 4682–4688.

[58] Wang, L.; Yang, Z. Z.; Samarakoon, W. S.; Zhou, Y. D.; Bowden, M. E.; Zhou, H.; Tao, J. H.; Zhu, Z. H.; Lahiri, N.; Droubay, T. C. et al. Spontaneous lithiation of binary oxides during epitaxial growth on $LiCoO_2$. *Nano Lett.* **2022**, *22*, 5530–5537.

[59] Xia, J.; Zhang, N.; Yang, Y. J.; Chen, X.; Wang, X.; Pan, F.; Yao, J. N. Lanthanide contraction builds better high-voltage $LiCoO_2$ batteries. *Adv. Funct. Mater.* **2023**, *33*, 2212869.

[60] Hu, B.; Lou, X. B.; Li, C.; Geng, F. S.; Zhao, C.; Wang, J. Y.; Shen, M.; Hu, B. W. Reversible phase transition enabled by binary Ba and Ti-based surface modification for high voltage $LiCoO_2$ cathode. *J. Power Sources* **2019**, *438*, 226954.

[61] Cheng, J. H.; Pan, C. J.; Nithya, C.; Thirunakaran, R.; Gopukumar, S.; Chen, C. H.; Lee, J. F.; Chen, J. M.; Sivashanmugam, A.; Hwang, B. J. Effect of Mg doping on the local structure of $LiMg_yCo_{1-y}O_2$ cathode material investigated by X-ray absorption spectroscopy. *J. Power Sources* **2014**, *252*, 292–297.

[62] Umair, M.; Nazir, G.; Murtaza, G.; Elamin, N. Y.; Muhammad, N.; Amin, M. A.; Somaily, H. H. Synthesis and characterization of Al and Zr-dual-doped lithium cobalt oxide cathode for Li-ion batteries using a facile hydrothermal approach. *Colloids Surf. A: Physicochem. Eng. Aspects* **2022**, *641*, 128493.

[63] Kong, W. J.; Wong, D.; An, K.; Zhang, J. C.; Chen, Z. H.; Schulz, C.; Xu, Z. J.; Liu, X. F. Stabilizing the anionic redox in 4.6 V $LiCoO_2$ cathode through adjusting oxygen magnetic moment. *Adv. Funct. Mater.* **2022**, *32*, 2202679.

[64] Tan, X. H.; Chen, Z. F.; Liu, T. C.; Zhang, Y. X.; Zhang, M. J.; Li, S. N.; Chu, W. G.; Liu, K.; Yang, P. H.; Pan, F. Imitating architectural mortise-tenon structure for stable Ni-rich layered cathodes. *Adv. Mater.* **2023**, *35*, 2301096.

[65] Fan, X. M.; Ou, X.; Zhao, W. G.; Liu, Y.; Zhang, B.; Zhang, J. F.; Zou, L. F.; Seidl, L.; Li, Y. Z.; Hu, G. R. et al. *In situ* inorganic conductive network formation in high-voltage single-crystal Ni-rich cathodes. *Nat. Commun.* **2021**, *12*, 5320.

[66] Zou, L. H.; Zhang, Y.; Wang, F.; Zhou, B. L.; Wang, Z. Y. Improving the cycle performance of $LiNi_{0.5}Co_{0.3}Mn_{0.2}O_2$ cathode material for lithium-ion batteries by carbon coating. *Integr. Ferroelectr.* **2013**, *147*, 103–109.

[67] Ruff, Z.; Coates, C. S.; Märker, K.; Mahadevegowda, A.; Xu, C.; Penrod, M. E.; Ducati, C.; Grey, C. P. O3 to O1 phase transitions in highly delithiated NMC811 at elevated temperatures. *Chem. Mater.* **2023**, *35*, 4979–4987.

[68] Kong, W. J.; Zhang, J. C.; Wong, D.; Yang, W. Y.; Yang, J. B.; Schulz, C.; Liu, X. F. Tailoring Co3d and O2p band centers to inhibit oxygen escape for stable 4.6 V $LiCoO_2$ cathodes. *Angew. Chem., Int. Ed.* **2021**, *60*, 27102–27112.

[69] Kim, S.; Cho, W.; Zhang, X. B.; Oshima, Y.; Choi, J. W. A stable lithium-rich surface structure for lithium-rich layered cathode materials. *Nat. Commun.* **2016**, *7*, 13598.

[70] Rozier, P.; Tarascon, J. M. Review-Li-rich layered oxide cathodes for next-generation Li-ion batteries: Chances and challenges. *J. Electrochem. Soc.* **2015**, *162*, A2490–A2499.

[71] Koichi, N.; Chie, S.; Shoji, Y. Synthesis of solid solutions in a system of $LiCoO_2$-Li_2MnO_3 for cathode materials of secondary lithium batteries. *Chem. Lett.* **1997**, *26*, 725–726.

[72] Yi, T. F.; Tao, W.; Chen, B.; Zhu, Y. R.; Yang, S. Y.; Xie, Y. High-performance $xLi_2MnO_3 \cdot (1-x)LiMn_{1/3}Co_{1/3}Ni_{1/3}O_2$ (0.1 x 0.5) as cathode material for lithium-ion battery. *Electrochim. Acta* **2016**, *188*, 686–695.

[73] Liu, Q. M.; Zhu, H. L.; Liu, J.; Liao, X. W.; Tang, Z. L.; Zhou, C. K.; Yuan, M. M.; Duan, J. F.; Li, L. J.; Chen, Z. Y. High-performance lithium-rich layered oxide material: Effects of preparation methods on microstructure and electrochemical properties. *Materials* **2020**, *13*, 334.

[74] Luo, D.; Cui, J. X.; Zhang, B. K.; Fan, J. M.; Liu, P. Z.; Ding, X. K.; Xie, H. X.; Zhang, Z. H.; Guo, J. J.; Pan, F. et al. Ti-based surface integrated layer and bulk doping for stable voltage and long life of Li-rich layered cathodes. *Adv. Funct. Mater.* **2021**, *31*, 2009310.

[75] Shao, Q. N.; Gao, P. Y.; Yan, C. H.; Gao, M. X.; Du, W. B.; Chen, J.; Yang, Y. X.; Gan, J. T.; Wu, Z. J.; Zhang, C. Y. et al. A redox couple strategy enables long-cycling Li- and Mn-rich layered oxide cathodes by suppressing oxygen release. *Adv. Mater.* **2022**, *34*, 2108543.

[76] Song, J.; Ning, F. H.; Zuo, Y. X.; Li, A.; Wang, H. C.; Zhang, K.; Yang, T. H.; Yang, Y. L.; Gao, C.; Xiao, W. K. et al. Entropy stabilization strategy for enhancing the local structural adaptability of Li-rich cathode materials. *Adv. Mater.* **2023**, *35*, 2208726.

[77] Yang, X. X.; Wang, S. N.; Han, D. Z.; Wang, K.; Tayal, A.; Baran, V.; Missyul, A.; Fu, Q.; Song, J. X.; Ehrenberg, H. et al. Structural origin of suppressed voltage decay in single-crystalline Li-rich layered $Li[Li_{0.2}Ni_{0.2}Mn_{0.6}]O_2$ cathodes. *Small* **2022**, *18*, 2201522.

[78] Boivin, E.; Guerrini, N.; House, R. A.; Lozano, J. G.; Jin, L. Y.; Rees, G. J.; Somerville, J. W.; Kuss, C.; Roberts, M. R.; Bruce, P. G. The role of Ni and Co in suppressing O-loss in Li-rich layered cathodes. *Adv. Funct. Mater.* **2021**, *31*, 2003660.

[79] Chai, K.; Zhang, J. C.; Li, Q. Y.; Wong, D.; Zheng, L. R.; Schulz, C.; Bartkowiak, M.; Smirnov, D.; Liu, X. F. Facilitating reversible cation migration and suppressing O_2 escape for high performance Li-rich oxide cathodes. *Small* **2022**, *18*, 2201014.

[80] Zheng, H. F.; Zhang, C. Y.; Zhang, Y. G.; Lin, L.; Liu, P. F.; Wang, L. S.; Wei, Q. L.; Lin, J.; Sa, B.; Xie, Q. S. et al. Manipulating the local electronic structure in Li-rich layered cathode towards superior electrochemical performance. *Adv. Funct. Mater.* **2021**, *31*, 2100783.

[81] Huang, J. P.; Ouyang, B.; Zhang, Y. Q.; Yin, L.; Kwon, D. H.; Cai, Z. J.; Lun, Z.; Zeng, G. B.; Balasubramanian, M.; Ceder, G. Inhibiting collective cation migration in Li-rich cathode materials as a strategy to mitigate voltage hysteresis. *Nat. Mater.* **2023**, *22*, 353–361.

[82] Ding, X.; Li, Y. X.; Wang, S.; Dong, J. M.; Yasmin, A.; Hu, Q.; Wen, Z. Y.; Chen, C. H. Towards improved structural stability and electrochemical properties of a Li-rich material by a strategy of double gradient surface modification. *Nano Energy* **2019**, *61*, 411–419.

[83] Hy, S.; Felix, F.; Rick, J.; Su, W. N.; Hwang, B. J. Direct *in situ* observation of Li_2O evolution on Li-rich high-capacity cathode material, $Li[Ni_xLi_{(1-2x)/3}Mn_{(2-x)/3}]O_2$ ($0 \le x \le 0.5$). *J. Am. Chem. Soc.* **2014**, *136*, 999–1007.

[84] Luo, K.; Roberts, M. R.; Hao, R.; Guerrini, N.; Pickup, D. M.; Liu, Y. S.; Edström, K.; Guo, J. H.; Chadwick, A. V.; Duda, L. C. et al.

Charge-compensation in 3d-transition-metal-oxide intercalation cathodes through the generation of localized electron holes on oxygen. *Nat. Chem.* **2016**, *8*, 684–691.

[85] Hua, W. B.; Wang, S. N.; Knapp, M.; Leake, S. J.; Senyshyn, A.; Richter, C.; Yavuz, M.; Binder, J. R.; Grey, C. P.; Ehrenberg, H. et al. Structural insights into the formation and voltage degradation of lithium- and manganese-rich layered oxides. *Nat. Commun.* **2019**, *10*, 5365.

[86] Hua, W. B.; Yang, X. X.; Casati, N. P. M.; Liu, L. J.; Wang, S. N.; Baran, V.; Knapp, M.; Ehrenberg, H.; Indris, S. Probing thermally-induced structural evolution during the synthesis of layered Li-, Na-, or K-containing 3d transition-metal oxides. *eScience* **2022**, *2*, 183–191.

[87] Zhang, C. X.; Wei, B.; Wang, M. Y.; Zhang, D. T.; Uchiyama, T.; Liang, C. P.; Chen, L. B.; Uchimoto, Y.; Zhang, R. F.; Wang, P. et al. Regulating oxygen covalent electron localization to enhance anionic redox reversibility of lithium-rich layered oxide cathodes. *Energy Storage Mater.* **2022**, *46*, 512–522.

[88] Chong, S. K.; Liu, Y. N.; Yan, W. W.; Chen, Y. Z. Effect of valence states of Ni and Mn on the structural and electrochemical properties of $Li_{1.2}Ni_xMn_{0.8-x}O_2$ cathode materials for lithium-ion batteries. *RSC Adv.* **2016**, *6*, 53662–53668.

[89] Kim, U. H.; Park, G. T.; Son, B. K.; Nam, G. W.; Liu, J.; Kuo, L. Y.; Kaghazchi, P.; Yoon, C. S.; Sun, Y. K. Heuristic solution for achieving long-term cycle stability for Ni-rich layered cathodes at full depth of discharge. *Nat. Energy* **2020**, *5*, 860–869.

[90] Mao, D. D.; Tan, X. H.; Fan, Z. W.; Song, L. T.; Zhang, Y. X.; Zhang, P.; Su, S.; Liu, G. Y.; Wang, H. F.; Chu, W. G. Unveiling the roles of trace Fe and F Co-doped into high-Ni Li-rich layered oxides in performance improvement. *ACS Appl. Mater. Interfaces* **2023**, *15*, 10774–10784.

[91] Shen, K.; Xu, X. J.; Tang, Y. P. Recent progress of magnetic field application in lithium-based batteries. *Nano Energy* **2022**, *92*, 106703.

[92] Han, Y. K.; Lei, Y. K.; Ni, J.; Zhang, Y. C.; Geng, Z.; Ming, P. W.; Zhang, C. M.; Tian, X. R.; Shi, J. L.; Guo, Y. G. et al. Single-crystalline cathodes for advanced Li-ion batteries: Progress and challenges. *Small* **2022**, *18*, 2107048.

[93] Jing, Z. W.; Wang, S. N.; Fu, Q.; Baran, V.; Tayal, A.; Casati, N. P. M.; Missyul, A.; Simonelli, L.; Knapp, M.; Li, F. J. et al. Architecting "Li-rich Ni-rich" core-shell layered cathodes for high-energy Li-ion batteries. *Energy Storage Mater.* **2023**, *59*, 102775.

[94] Dahn, J. R.; von Sacken, U.; Michal, C. A. Structure and electrochemistry of $Li_{1\pm y}NiO_2$ and a new Li_2NiO_2 phase with the $Ni(OH)_2$ structure. *Solid State Ionics* **1990**, *44*, 87–97.

[95] Dutta, G.; Manthiram, A.; Goodenough, J. B.; Grenier, J. C. Chemical synthesis and properties of $Li_{1-\delta-x}Ni_{1+\delta}O_2$ and $Li[Ni_2]O_4$. *J. Solid State Chem.* **1992**, *96*, 123–131.

[96] Bruce, P. G.; Lisowska-Oleksiak, A.; Saidi, M. Y.; Vincent, C. A. Vacancy diffusion in the intercalation electrode $Li_{1-x}NiO_2$. *Solid State Ionics* **1992**, *57*, 353–358.

[97] Cui, Z. H.; Guo, Z. Z.; Manthiram, A. Assessing the intrinsic roles of key dopant elements in high-nickel layered oxide cathodes in lithium-based batteries. *Adv. Energy Mater.* **2023**, *13*, 2203853.

[98] Yuwono, R. A.; Wang, F. M.; Wu, N. L.; Chen, Y. C.; Chen, H.; Chen, J. M.; Haw, S. C.; Lee, J. F.; Xie, R. K.; Sheu, H. S. et al. Evaluation of $LiNiO_2$ with minimal cation mixing as a cathode for Li-ion batteries. *Chem. Eng. J.* **2023**, *456*, 141065.

[99] Kim, M.; Zou, L. F.; Son, S. B.; Bloom, I. D.; Wang, C. M.; Chen, G. Y. Improving $LiNiO_2$ cathode performance through particle design and optimization. *J. Mater. Chem. A* **2022**, *10*, 12890–12899.

[100] Goonetilleke, D.; Mazilkin, A.; Weber, D.; Ma, Y.; Fauth, F.; Janek, J.; Brezesinski, T.; Bianchini, M. Single step synthesis of W-modified $LiNiO_2$ using an ammonium tungstate flux. *J. Mater. Chem. A* **2022**, *10*, 7841–7855.

[101] Geng, C. X.; Rathore, D.; Heino, D.; Zhang, N.; Hamam, I.; Zaker, N.; Botton, G. A.; Omessi, R.; Phattharasupakun, N.; Bond, T. et al. Mechanism of action of the tungsten dopant in $LiNiO_2$ positive electrode materials. *Adv. Energy Mater.* **2022**, *12*, 2103067.

[102] Liu, Z. C.; Zhen, H. H.; Kim, Y.; Liang, C. D. Synthesis of $LiNiO_2$ cathode materials with homogeneous Al doping at the atomic level. *J. Power Sources* **2011**, *196*, 10201–10206.

[103] Cho, J.; Kim, T. J.; Kim, Y. J.; Park, B. High-performance ZrO_2-coated $LiNiO_2$ cathode materials. *Electrochem. Solid-State Lett.* **2001**, *4*, A159–A161.

[104] Kang, J.; Han, B. First-principles study on the thermal stability of $LiNiO_2$ materials coated by amorphous Al_2O_3 with atomic layer thickness. *ACS Appl. Mater. Interfaces* **2015**, *7*, 11599–11603.

[105] Mohan, P.; Kalaignan, G. P. Electrochemical behaviour of surface modified SiO_2-coated $LiNiO_2$ cathode materials for rechargeable lithium-ion batteries. *J. Nanosci. Nanotechnol.* **2013**, *13*, 2765–2770.

[106] Kaneda, H.; Furuichi, Y.; Ikezawa, A.; Arai, H. Effects of aluminum substitution in nickel-rich layered $LiNi_xAl_{1-x}O_2$ (x = 0.92, 0.95) positive electrode materials for Li-ion batteries on high-rate cycle performance. *J. Mater. Chem. A* **2021**, *9*, 21981–21994.

[107] Zhang, Q. H.; Su, Y. W.; Shi, Z. X.; Yang, X. Z.; Sun, J. Y. Artificial interphase layer for stabilized Zn anodes: Progress and prospects. *Small* **2022**, *18*, 2203583.

[108] Yu, T.; Yang, H. C.; Cheng, H. M.; Li, F. Theoretical progress of 2D six-membered-ring inorganic materials as anodes for non-lithium-ion batteries. *Small* **2022**, *18*, 2107868.

[109] Xu, J. K.; Lei, J. F.; Ming, N. N.; Zhang, C. T.; Huo, K. F. Rational design of wood-structured thick electrode for electrochemical energy storage. *Adv. Funct. Mater.* **2022**, *32*, 2204426.

[110] Xu, G. Y.; Zhu, C. Y.; Gao, G. Recent progress of advanced conductive metal-organic frameworks: Precise synthesis, electrochemical energy storage applications, and future challenges. *Small* **2022**, *18*, 2203140.

[111] Wu, M. C.; Zheng, W. Y.; Hu, X.; Zhan, F. Y.; He, Q. Q.; Wang, H. Y.; Zhang, Q. C.; Chen, L. Y. Exploring 2D energy storage materials: Advances in structure, synthesis, optimization strategies, and applications for monovalent and multivalent metal-ion hybrid capacitors. *Small* **2022**, *18*, 2205101.

[112] Wang, Z.; Pan, F.; Zhao, Q.; Lv, M. L.; Zhang, B. The application of covalent organic frameworks in lithium-sulfur batteries: A mini review for current research progress. *Front. Chem.* **2022**, *10*, 1055649.

[113] Ren, X. H.; Wang, H. Y.; Chen, J.; Xu, W. L.; He, Q. Q.; Wang, H. Y.; Zhan, F. Y.; Chen, S. W.; Chen, L. Y. Emerging 2D copper-based materials for energy storage and conversion: A review and perspective. *Small* **2023**, *19*, 2204121.

[114] Xie, L. J.; Tang, C.; Bi, Z. H.; Song, M. X.; Fan, Y. F.; Yan, C.; Li, X. M.; Su, F. Y.; Zhang, Q.; Chen, C. M. Hard carbon anodes for next-generation Li-ion batteries: Review and perspective. *Adv. Energy Mater.* **2021**, *11*, 2101650.

[115] Shen, Y. F.; Qian, J. F.; Yang, H. X.; Zhong, F. P.; Ai, X. P. Chemically prelithiated hard-carbon anode for high power and high capacity Li-ion batteries. *Small* **2020**, *16*, 1907602.

[116] Zhuo, R. F.; Quan, W. W.; Huang, X. Z.; He, Q.; Sun, Z. G.; Zhang, Z. Y.; Wang, J. Well-dispersed tin nanoparticles encapsulated in amorphous carbon tubes as high-performance anode for lithium ion batteries. *Nanotechnology* **2021**, *32*, 145402.

[117] Xu, Z. W.; Wang, Y.; Liu, M. Y.; Sarwar, M. K.; Zhao, Y. X. Defects enriched cobalt molybdate induced by carbon dots for a high rate Li-ion battery anode. *Nanotechnology* **2022**, *33*, 075402.

[118] Permana, A. D. C.; Omar, A.; Gonzalez-Martinez, I. G.; Oswald, S.; Giebeler, L.; Nielsch, K.; Mikhailova, D. MOF-derived onion-like carbon with superior surface area and porosity for high performance lithium-ion capacitors. *Batt. Supercaps* **2022**, *5*, e202100353.

[119] Gao, C. W.; Jiang, Z. J.; Qi, S. B.; Wang, P. X.; Jensen, L. R.; Johansen, M.; Christensen, C. K.; Zhang, Y. F.; Ravnsbæk, D. B.; Yue, Y. Z. Metal-organic framework glass anode with an exceptional cycling-induced capacity enhancement for lithium-ion batteries. *Adv. Mater.* **2022**, *34*, 2110048.

[120] Zhao, L. F.; Hu, Z.; Lai, W. H.; Tao, Y.; Peng, J.; Miao, Z. C.; Wang, Y. X.; Chou, S. L.; Liu, H. K.; Dou, S. X. Hard carbon anodes: Fundamental understanding and commercial perspectives for Na-ion batteries beyond Li-ion and K-ion counterparts. *Adv. Energy Mater.* **2021**, *11*, 2002704.

[121] Ha, S.; Hyun, J. C.; Kwak, J. H.; Lim, H. D.; Yun, Y. S. Hierarchically nanoporous 3D assembly composed of functionalized onion-like graphitic carbon nanospheres for anode-minimized Li metal batteries. *Small* **2020**, *16*, 2003918.

[122] Chai, Y. J.; Du, Y. H.; Li, L.; Wang, N. Dual metal oxides interconnected by carbon nanotubes for high-capacity Li- and Na-ion batteries. *Nanotechnology* **2020**, *31*, 215402.

[123] Xie, Y. W.; Zhang, H. Y.; Yu, J. L.; Liu, Z. J.; Zhang, S. S.; Shao, H. Y.; Cao, Y. L.; Huang, X. F.; Li, S. K. A novel dendrite-free lithium metal anode via oxygen and boron codoped honeycomb carbon skeleton. *Small* **2022**, *18*, 2104876.

[124] Liu, R. Q.; Xu, S. S.; Shao, X. X.; Wen, Y.; Shi, X. R.; Hu, J.; Yang, Z. Carbon coating on metal oxide materials for electrochemical energy storage. *Nanotechnology* **2021**, *32*, 502004.

[125] Olsson, E.; Yu, J. L.; Zhang, H. Y.; Cheng, H. M.; Cai, Q. Atomic-scale design of anode materials for alkali metal (Li/Na/K)-ion batteries: Progress and perspectives. *Adv. Energy Mater.* **2022**, *12*, 2200662.

[126] Chen, K. H.; Goel, V.; Namkoong, M. J.; Wied, M.; Müller, S.; Wood, V.; Sakamoto, J.; Thornton, K.; Dasgupta, N. P. Enabling 6C fast charging of Li-ion batteries with graphite/hard carbon hybrid anodes. *Adv. Energy Mater.* **2021**, *11*, 2003336.

[127] Xu, H. R.; Zhao, L. L.; Liu, X. M.; Huang, Q. S.; Wang, Y. Q.; Hou, C. X.; Hou, Y. Y.; Wang, J.; Dang, F.; Zhang, J. T. Metal-organic-framework derived core–shell N-doped carbon nanocages embedded with cobalt nanoparticles as high-performance anode materials for lithium-ion batteries. *Adv. Funct. Mater.* **2020**, *30*, 2006188.

[128] Lee, M. J.; Lee, K.; Lim, J.; Li, M. C.; Noda, S.; Kwon, S. J.; DeMattia, B.; Lee, B.; Lee, S. W. Outstanding low-temperature performance of structure-controlled graphene anode based on surface-controlled charge storage mechanism. *Adv. Funct. Mater.* **2021**, *31*, 2009397.

[129] Zhang, F.; Zhu, W. Q.; Li, T. T.; Yuan, Y.; Yin, J.; Jiang, J. H.; Yang, L. S. Advances of synthesis methods for porous silicon-based anode materials. *Front. Chem.* **2022**, *10*, 889563.

[130] Song, L. T.; Zhao, T. Q.; Tan, X. H.; Mao, D. D.; Su, S.; Fan, Z. W.; Chu, W. G. Biomass-derived hierarchically porous (nitrogen, phosphorus) Co-doped SiO_x/C composite nanosheet architectures for superior lithium storage and ultra-long cycle performance. *Batt. Supercaps* **2022**, *5*, e202100350.

[131] McBrayer, J. D.; Rodrigues, M. T. F.; Schulze, M. C.; Abraham, D. P.; Apblett, C. A.; Bloom, I.; Carroll, G. M.; Colclasure, A. M.; Fang, C.; Harrison, K. L. et al. Calendar aging of silicon-containing batteries. *Nat. Energy* **2021**, *6*, 866–872.

[132] Guo, X. T.; Xu, H. Y.; Li, W. T.; Liu, Y. Y.; Shi, Y. X.; Li, Q.; Pang, H. Embedding atomically dispersed iron sites in nitrogen-doped carbon frameworks-wrapped silicon suboxide for superior lithium storage. *Adv. Sci.* **2023**, *10*, 2206084.

[133] Tan, W.; Wang, L. N.; Lu, Z. G.; Yang, F.; Xu, Z. H. A hierarchical Si/C nanocomposite of stable conductive network formed through thermal phase separation of asphaltenes for high-performance Li-ion batteries. *Small* **2022**, *18*, 2203102.

[134] Cai, Y. F.; Liu, C. X.; Yu, Z. A.; Ma, W. C.; Jin, Q.; Du, R. C.; Qian, B. Y.; Jin, X. X.; Wu, H. M.; Zhang, Q. H. et al. Slidable and highly ionic conductive polymer binder for high-performance Si anodes in lithium-ion batteries. *Adv. Sci.* **2023**, *10*, 2205590.

[135] Xiao, Z. X.; Lin, X. Q.; Zhang, C. X.; Shen, J. Q.; Zhang, R. R.; He, Z. Y.; Lin, Z. K.; Jiang, H. R.; Wei, F. Insights into the coating integrity and its effect on the electrochemical performance of core–shell structure SiO_x@C composite anodes. *Small Methods* **2023**, *7*, 2201623.

[136] Tian, Y. F.; Li, G.; Xu, D. X.; Lu, Z. Y.; Yan, M. Y.; Wan, J.; Li, J. Y.; Xu, Q.; Xin, S.; Wen, R. et al. Micrometer-sized $SiMg_yO_x$ with stable internal structure evolution for high-performance Li-ion battery anodes. *Adv. Mater.* **2022**, *34*, 2200672.

[137] Oh, M. G.; Kwak, S.; An, K.; Tran, Y. H. T.; Kang, D. G.; Park, S. J.; Lim, G.; Kim, K.; Lee, Y. S.; Song, S. W. Perfluoro macrocyclic ether as an ambifunctional additive for high-performance SiO and nickel 88%-based high-energy Li-ion battery. *Adv. Funct. Mater.* **2023**, *33*, 2212890.

[138] Pan, S. S.; Yang, L. P.; Su, P. P.; Zhang, H. T.; Zhang, S. J. Robust multiscale electron/ion transport and enhanced structural stability in SiO_x semi-solid anolytes enabled by trifunctional artificial interfaces for high-performance Li-ion slurry flow batteries. *Small* **2022**, *18*, 2202139.

[139] Im, J.; Kwon, J. D.; Kim, D. H.; Yoon, S.; Cho, K. Y. P-doped SiO_x/Si/SiO_x sandwich anode for Li-ion batteries to achieve high initial coulombic efficiency and low capacity decay. *Small Methods* **2022**, *6*, 2101052.

[140] Lee, H. A.; Shin, M.; Kim, J.; Choi, J. W.; Lee, H. Designing adaptive binders for microenvironment settings of silicon anode particles. *Adv. Mater.* **2021**, *33*, 2007460.

[141] Cao, Z.; Zheng, X. Y.; Qu, Q. T.; Huang, Y. H.; Zheng, H. H. Electrolyte design enabling a high-safety and high-performance Si anode with a tailored electrode-electrolyte interphase. *Adv. Mater.* **2021**, *33*, 2103178.

[142] Collins, G. A.; Kilian, S.; Geaney, H.; Ryan, K. M. A nanowire nest structure comprising copper silicide and silicon nanowires for lithium-ion battery anodes with high areal loading. *Small* **2021**, *17*, 2102333.

[143] Chae, S.; Xu, Y. B.; Yi, R.; Lim, H. S.; Velickovic, D.; Li, X. L.; Li, Q. Y.; Wang, C. M.; Zhang, J. G. A micrometer-sized silicon/carbon composite anode synthesized by impregnation of petroleum pitch in nanoporous silicon. *Adv. Mater.* **2021**, *33*, 2103095.

[144] Ren, Y.; Xiang, L. Z.; Yin, X. C.; Xiao, R.; Zuo, P. J.; Gao, Y. Z.; Yin, G. P.; Du, C. Y. Ultrathin Si nanosheets dispersed in graphene matrix enable stable interface and high rate capability of anode for lithium-ion batteries. *Adv. Funct. Mater.* **2022**, *32*, 2110046.

[145] Hernandha, R. F. H.; Rath, P. C.; Umesh, B.; Patra, J.; Huang, C. Y.; Wu, W. W.; Dong, Q. F.; Li, J.; Chang, J. K. Supercritical CO_2-assisted SiO_x/carbon multi-layer coating on Si anode for lithium-ion batteries. *Adv. Funct. Mater.* **2021**, *31*, 2104135.

[146] Su, Y. X.; Feng, X.; Zheng, R. B.; Lv, Y. Y.; Wang, Z. Y.; Zhao, Y.; Shi, L. Y.; Yuan, S. Binary network of conductive elastic polymer constraining nanosilicon for a high-performance lithium-ion battery. *Acs Nano* **2021**, *15*, 14570–14579.

[147] Li, Z. H.; Wu, G.; Yang, Y. J.; Wan, Z. W.; Zeng, X. M.; Yan, L. J.; Wu, S. X.; Ling, M.; Liang, C. D.; Hui, K. N. et al. An ion-conductive grafted polymeric binder with practical loading for silicon anode with high interfacial stability in lithium-ion batteries. *Adv. Energy Mater.* **2022**, *12*, 2201197.

[148] Jiang, M. M.; Chen, J. L.; Zhang, Y. B.; Song, N.; Jiang, W.; Yang, J. P. Assembly: A key enabler for the construction of superior silicon-based anodes. *Adv. Sci.* **2022**, *9*, 2203162.

[149] Moon, J.; Lee, H. C.; Jung, H.; Wakita, S.; Cho, S.; Yoon, J.; Lee, J.; Ueda, A.; Choi, B.; Lee, S. et al. Interplay between electrochemical reactions and mechanical responses in silicon-graphite anodes and its impact on degradation. *Nat. Commun.* **2021**, *12*, 2710.